Climate Dynamics
https://doi.org/10.1007/s00382-021-05880-z

Changing status of tropical cyclones over the north Indian Ocean

Medha Deshpande[1] · Vineet Kumar Singh[1,2] · Mano Kranthi Ganadhi[1,3] · M. K. Roxy[1] · R. Emmanuel[1,3] · Umesh Kumar[1,4]

Received: 1 October 2020 / Accepted: 4 July 2021

Abstract
Climatologically, the frequency of tropical cyclones (TCs) in the Bay of Bengal (BoB) is higher relative to that over the Arabian Sea (ARB). However, recent years exhibit a greater number of TCs forming in the ARB than in the BoB. During the study period (1982–2019), a significant increasing trend in the intensity, frequency, and duration of cyclonic storms (CS) and very severe CS (VSCS) is observed over the ARB. There is a 52% increase in the frequency of CS during the recent epoch (2001–2019) in the ARB, while there is a decrease of 8% in the BoB. Over the ARB, increment in CS duration is 80% and VSCS is almost threefold in the recent epoch as compared to the past epoch (1982–2000). Also, lifetime maximum intensity and accumulated cyclone energy have increased over the ARB implying an increase in the strength of TCs. The increase in TC duration over the ARB is prominent during May, June, and October and a decrease over the BoB is noted during November. The increase in the duration of TCs in the ARB is associated with an increase in mid-level relative humidity and column averaged (950-150 hPa) moist static energy, which is significantly correlated to an increase in sea surface temperatures and tropical cyclone heat potential in the basin. In the recent epoch, TC genesis is observed at lower latitudes ($< 8°$ N), which is another factor contributing to longer durations of TCs. This increases the probability of TC intensification with the support from other favourable environmental parameters. Significant changes in TC tracks are also noted in May, June, and October due to changes in steering currents.

Keywords Tropical cyclones · Climate change · North Indian Ocean · Bay of Bengal · Arabian Sea

1 Introduction

Tropical cyclones (TCs) formed over the north Indian Ocean (NIO) cause enormous devastation in the densely populated area. As per India Meteorological Department (IMD), the TCs are characterized based on the 3-min sustained maximum wind speed (Table 1). On average, four or five systems reach at least CS stage per year. NIO is divided into two basins: the Bay of Bengal (BoB) and the Arabian Sea (ARB). The ocean–atmospheric conditions make BoB more conducive for TC formation than ARB. On average, three to four TCs form per year in the BoB (Alam et al. 2003). BoB TC activity is 4 times higher than ARB (Dube et al. 1997; Singh et al. 2001). Recently, 2019 was the most active year for NIO with eight numbers of TCs; out of which five formed in the ARB. Also, in 2018 out of seven TCs three formed in ARB. Apart from the greater number of TCs over ARB in recent years, a rare, back-to-back ESCSs occurred within a single month, for the first time in 2015. TC Chapala and Megha formed one after another in November 2015 with a maximum intensity of 135 and 110 knots (69.4 and 56.6 m s^{-1}), respectively. Also, in October 2019, TC Kyarr and Maha existed simultaneously in ARB with a maximum intensity of 130 and 100 knots (66.9 and 51.4 m s^{-1}). Very recently (June 2020), SCS Nisarga formed over ARB had a landfall on the Maharashtra coast near Mumbai. This was the first time in the recorded history that a TC made landfall at the Maharashtra coast in June. In 2021, ESCS Tauktae

✉ Medha Deshpande
medha_d@tropmet.res.in

[1] Indian Institute of Tropical Meteorology, Ministry of Earth Sciences, Dr. Homi Bhabha Road, Pashan, Pune 411 008, India

[2] Department of Atmospheric and Space Sciences, Savitribai Phule Pune University, Pune, Maharashtra, India

[3] School of Environmental and Earth Sciences, KBC North Maharashtra University, Jalgaon, Maharashtra, India

[4] Department of Earth and Atmospheric Sciences, National Institute of Technology, Rourkela, Odisha, India

Published online: 17 July 2021

Table 1 Classification of cyclonic disturbances in the north Indian ocean by India Meteorological Department based on maximum sustained wind speed in knot (Kmph)

System	Wind speed knot (Kmph)
Low pressure area	< 17 (< 31)
Depression	17–27 (31–49)
Deep depression (DD)	28–33 (50–61)
Cyclonic storm (CS)	34–47 (62–88)
Severe cyclonic storm (SCS)	48–63 (89–117)
Very severe cyclonic storm (VSCS)	64–89 (118–166)
Extremely severe cyclonic storm (ESCS)	90–119 (167–221)
Super cyclonic storm (SuCS)	≥ 120 (≥ 222)

in ARB was one of the strongest TC to ever affect the four states along the west coast of India. Though climatologically TC frequency is less over the NIO, particularly in ARB, these recent decade events raise a question: are the characteristics of TCs changing in the NIO? It is of great importance to understand the changes in the TC characteristics like the frequency, intensity, and track over NIO.

Past studies have investigated the changes in TC frequency and intensity over various basins. An increase in hurricane frequency over the north Atlantic (Goldenberg et al. 2001) and the north Pacific (Emanuel 2005) is reported by many researchers. Emanuel (2005) showed an increasing trend in TC lifetime and intensity (1949–2003) over the north Pacific is correlated with tropical Sea surface temperature (SST). Webster et al. (2005) reported a steady increase in the number and percentage of intense TCs across all basins for the period 1970–2004. Elsner et al. (2008) confirmed an increase in the intensity of strongest TCs over the globe, during the satellite era (1981–2006). Analysis of NIO TC trends, specifically considering BoB and ARB separately, are limited. Based on 122 years (1877–1998) of data, Singh et al. (2001) concluded that the TC frequency over BoB has increased in May and November with an increase in intensification rate in November. Balaguru et al. (2014) showed an increase in the intensity of major cyclonic storms over BoB (wind speed greater than 49 m s^{-1}) during the post-monsoon season (1981–2010). They attributed this to an increase in SST, ocean heat content, and atmospheric convective instability. On the contrary, Srivastav et al. (2000) showed a decreasing trend in TCs frequency over ARB and BoB. They linked this to the weakening of Hadley circulation due to upper tropospheric warming. Deo and Ganer (2015) reported an increasing trend in the length of TC season (1979–2008) with a prominent increase in pre-monsoon season (March–April–May). Balaji et al. (2018) also showed an increase in the frequency of NIO VSCSs (1981–2014). Whereas, Mohapatra et al. (2014) found no significant trend in annual frequency of CS or SCS over ARB for the period 1961–2010. Singh et al. (2000) reported no significant long-term linear trend (1891–2008) in ARB TC frequency. From1979 onwards there is an increase in the number of TCs, over ARB (Deo et al. 2011; Evan et al. 2011; Rajeevan et al. 2013; Singh et al. 2019a, b). The increasing trend of cyclogenesis over the ARB is mainly attributed to an increase in SST (Deo et al. 2011), ocean heat content (Rajeevan et al. 2013), and a decrease in wind shear (Deo et al. 2011; Evan et al. 2011; Rajeevan et al. 2013). Evan et al. (2011) argued that the decrease in wind shear is associated with a simultaneous upward trend in anthropogenic black carbon and sulphate aerosols. However, Mohapatra and Vijay Kumar (2017) showed that the accumulated cyclone energy (ACE), is decreasing in the post-monsoon season (1990–2013). Previous studies also reported an epochal variability in frequency and intensity of TCs over BoB and ARB (Evan and Camargo 2011; Ng and Chan 2012; Baburaj et al. 2020).

In general, NIO TC frequency and intensity study considering ARB and BoB activity separately is limited. In some studies, pre-satellite data is included in the analysis which is not reliable (Klotzbach 2006) and also in other studes the recent data (after 2010) is not included. The focus of previous studies was to discuss the trends in TC frequency and intensity. Along with frequency and intensity; the changes in locations of genesis and tracks involve societal importance. Recently, using data for 1980–2018, Murakami et al. (2020) detected the changes in global distribution and spatial patterns of TC occurrence. They reported no trend in global TC frequency, but a decreasing trend over the south Indian ocean, western north Pacific, north-east coast of Australia, and an increasing trend in ARB, central Pacific, and north Atlantic basins. Balaji et al. (2018) showed that in the BoB, the genesis of VSCS has shifted 2.3° eastwards. Their study was limited to the genesis of VSCS in BoB. However, there is no in-depth understanding of changes in the genesis location of TCs (including all TCs, CS, and above). Few recent studies showed a decadal variation in the track of TCs in ARB and BoB, and changes in the landfall locations of TCs over Indian Ocean rim countries (Singh et al. 2019b; Bhatla et al. 2020). However, a thorough study on season-wise changes in TC tracks and the mechanism responsible for it is lacking. Further, climate models project an increase in the frequency of the ARB TCs by ~ 40% and a decrease in the frequency of the BoB TCs by ~ 30% in the global warming scenario (Murakami et al. 2013; Bell et al. 2020). The intensity of the TCs over the north Indian Ocean is also projected to increase in a warming climate (Bhatia et al. 2018; Mittal et al. 2019; Knutson et al. 2020; Reddy et al. 2021). In view of these factors, we examined the changes in TC activity over BoB and ARB separately

in terms of frequency, duration, month-wise distribution, genesis locations, and tracks for 38 years period (1982–2019). We also explored the mechanism responsible for observed changes using satellites and reanalysis data.

2 Data and methodology

In this study, TC frequency, intensity and track data are obtained from Joint Typhoon Warning Center (JTWC) (Chu et al. 2002). To minimize the impact of satellite-induced in-homogeneities, TCs before 1982 are not included. Consequently, the study period consists of 38 years of data from 1982 to 2019. Being a post geostationary satellite era, this period is most reliable without any missing TCs and with the best estimate of intensity for the NIO TCs, especially in the ARB (Mohapatra and Adhikary 2011). TCs that made landfall and moved into other basins are considered in their respective basin in which they have their genesis. Different terminologies are used in different basins to categorize the intensity of the TCs. In general, NIO CS intensity is equivalent to Tropical Storm in north Atlantic and north Pacific basin. Similarly, the NIO VSCS is equivalent to a hurricane in the north Atlantic and typhoons in the north Pacific basins. We considered the CS and VSCS categories of TC for the study. Here the frequency and duration of CS category includes the frequency and duration of TCs in CS and above category including VSCS. The duration of VSCS includes only the duration in which the TC was in VSCS and above category.

National Oceanic and Atmospheric Administration (NOAA) Optimum Interpolation sea surface temperature data set at a spatial resolution of 0.25° × 0.25° (Reynolds et al. 2007) and daily outgoing longwave radiation (OLR, Wm^{-2}) with a spatial resolution of 1° × 1° are used. Tropical cyclone heat potential (TCHP) is integrated heat content per unit area relative to 26 °C isotherm (Leipper and Volgenau 1972; Shay et al. 2000; Lin et al. 2008).

$$\mathrm{TCHP} = \rho C_p \int_0^{z26} (T - 26) dz \tag{1}$$

where ρ (1026 kg m^{-3}) is average upper ocean water density. C_p (4178 J kg^{-1} $°C^{-1}$) is the specific heat capacity of ocean water at constant pressure, and Z_{26} is the depth of 26 °C isotherm in the ocean. TCHP calculation is based on ocean sub-surface monthly temperature data (spatial resolution of 0.33° × 1°) obtained from NCEP-GODAS (available at https://psl.noaa.gov/).

ACE is calculated by summing the squares of the six-hourly maximum sustained surface wind speed (knot) during the duration when the system has a wind speed of 35 kt (18 m s^{-1}) or higher. ACE accounts for the combined strength and duration of TC and is proportional to its kinetic energy. The value is divided by 10^4 to make it easy to interpret (Camargo and Sobel 2005). ACE is estimated as

$$\mathrm{ACE} = 10^{-4} \sum \mathrm{v}^2 \tag{2}$$

where v is the maximum sustained wind speed in knots obtained from JTWC.

The translation speed of the cyclone is calculated using the six-hourly cyclone position data and then calculating the distance between the six-hourly locations along a great circle arc.

ERA5 monthly mean reanalysis data (wind, relative humidity, and relative vorticity) at a spatial resolution of 0.25° × 0.25° is utilized. The area considered for averaging is ARB (50°–80° E, 0°–25° N) and BoB (80°–100° E, 0°–25° N).

Genesis potential parameter (GPP) is used to identify the potential zone of cyclogenesis based on the thermodynamic and dynamic parameters. It is calculated using the methodology given by Kotal et al. (2009). This index was based on atmospheric parameters and didn't include any ocean parameters. Hence to include the effect of the ocean on the cyclogenesis a new index is defined by Suneeta and Sadhuram (2018) which incorporates both ocean and atmosphere parameters. The modified GPP (hereafter GPI) given by the following Eq. (3) is better correlated with the depression, cyclone, and severe cyclone frequency compared to the existing GPP (Suneeta and Sadhuram 2018).

$$\mathrm{GPI} = \mathrm{GPP} * \left(\frac{UOHC}{40}\right) \tag{3}$$

Here UOHC = Upper Ocean Heat Content (UOHC) also known as Tropical Cyclone Heat Potential (TCHP).

GPP is the Genesis Potential Parameter proposed by (Kotal et al. 2009).

$$\mathrm{GPP} = \frac{\xi_{850} \times M \times I}{S} \quad if \quad \xi_{850} > 0, M > 0 \quad and \quad I > 0 \tag{4}$$

$$= 0 \quad if \quad \xi_{850} \le 0, M \le 0 \quad or \quad I \le 0 \tag{5}$$

ξ_{850} = low-level relative vorticity at 850 hPa (10^{-5} s^{-1}); $M = \frac{[RH-40]}{30}$, RH is the middle tropospheric relative humidity average between 700 and 500 hPa; $I = (T_{850} - T_{500})°C$ is the middle tropospheric instability (Temperature difference between 850 and 500 hPa); S = Vertical wind shear of horizontal winds between 200 and 850 hPa.

The potential intensity (PI) is the theoretical limit to maximum achievable intensity by a TC. The PI of a TC is measured in terms of Vmax. It's computation is based on

Bister and Emanuel (2002) given by the following equation and detail about the calculation is available at (ftp://texmex.mit.edu/pub/emanuel/TCMAX).

$$(Vmax)^2 = \frac{C_K}{C_D}\frac{T_s}{T_0}(CAPE^* - CAPE)_m \tag{6}$$

where T_S is sea surface temperature (°C), T_O is outflow temperature, C_k is the surface enthalpy exchange coefficient, C_D is the drag coefficient, $\frac{C_k}{C_D}=0.9$ is the ratio of exchange coefficients, $CAPE^*$ is the convective available potential energy of airlifted from saturation at sea level in reference to the environmental sounding, and $CAPE$ is that of boundary layer air. Both quantities are evaluated near the radius of maximum wind.

Vertical wind shear of horizontal wind is defined as the magnitude of the vector difference between the upper-level and lower-level wind measured along the 200 hPa and 850 hPa pressure levels, respectively (Knaff et al. 2005).

Fluxes such as surface sensible heat and surface latent heat are obtained from monthly single level ERA5 high-resolution reanalysis data (Hersbach et al. 2020).The unit for both the fluxes is J m^{-2}. Recent paper by Pokhrel et al. (2020) evaluated the heat flux data from four reanalysis (NCEP-1, CFSR, ERA5 and MERRA) and two blended products (OAFlux and TropFlux) against the in situ observations (Moored bouys). They concluded that in general, ERA5 outperforms all other products (including OAflux) for most of the cases with the highest correlation, least RMSE, and most explained variance with respect to the in situ values. Considering these we are using the flux data from ERA5 in this study.

Moist static energy (MSE) is expressed as a sum of internal energy, potential energy, and latent heat energy (Neelin and Held 1987; Emanuel et al. 1994; Marquet 2015).

$$MSE = C_pT + gz + L_vq \tag{7}$$

where $C_p = 1.005$ kJ kg^{-1} K^{-1} is the specific heat capacity of dry air at constant pressure, T is the temperature, $L_v = 2256$ kJ kg^{-1} is the latent heat of condensation, q is specific humidity. Here MSE is averaged over the column (950-150 hPa levels).

Regression analysis is conducted to know the significance of the trend (p value) in the data set, where $p > 0.1$ not significant, $0.05 < p < 0.1$ marginally significant, $p < 0.05$ significant and $p < 0.01$ highly significant. This paper addresses statistically meaningful trends at a 5% level of significance (95% confidence level). ERA5, daily reanalysis wind data is used for computing steering wind (700–200 hPa) during TC. We utilized wind and OLR data during TC after removing the vortex to exclude the impact of the TC on the background large-scale flow. TC is removed based on Carl Schreck's methodology (Schreck et al. 2011) using a weighting function cantered on each storm's position. The storm's center is obtained from (Joint typhoon warning center) JTWC. The weighting function provided as

$$w(x,y) = 1 - \exp\left\{-\frac{r(x,y)^2}{2\left[R(2ln2)^{-1/2}\right]^2}\right\} \tag{8}$$

where r(x, y) is the distance from a given grid point to the tropical cyclone's center and R is the radius at half maximum of the weighting function. To remove the TC, the difference between the actual data and its climatological value at each location is multiplied by the weight from a given equation. At zero radius of the TC, all of the data above climatology is removed, and the removal fraction decreases with radius following the Gaussian function. Galarneau and Davis (2013) proposed a new TC removal technique. This methodology is adopted to decompose the wind fields into TC and Non-TC wind components. The TC components of stream function and velocity potential are defined as

$$\nabla^2\Psi = \begin{cases} \xi, (r \le \boldsymbol{r_o}) \\ 0, (r \ge \boldsymbol{r_o}) \end{cases} \quad \text{and} \quad \nabla^2\chi = \begin{cases} \delta, (r \le \boldsymbol{r_o}) \\ 0, (r \ge \boldsymbol{r_o}) \end{cases} \tag{9}$$

Here Ψ is the stream function, χ the velocity potential, ξ is the relative vorticity, δ is the divergence, ∇ is the two-dimensional gradient operator and r_o is the radius of TC. Using this Helmholtz equation, TC associated rotational and divergent wind components are calculated by the TC-associated stream function and velocity potential respectively. This Methodology removes all of the rotational and divergent wind fields inside the pre-determined domain.

3 Results and discussions

3.1 Changes in frequency, intensity, and duration of TCs

Figures 1a, b are histograms for CS and VSCS category TCs respectively. Out of 38 (1982–2019) years, during 6 years (1990, 1991, 2000, 2005, 2008, 2017) there were no CS over ARB whereas there was at least one CS over BoB except in 2001. Year 2001 was an exceptional year when not a single CS formed over BoB but 4 formed over ARB. In all 38 years period there was a TC over either BoB or ARB or over both the basins. In the majority of years, one or two TCs formed in ARB, whereas 3–4 formed in BoB. Intensification of TCs up to VSCS category is comparatively fewer in the ARB. Out of 38 years, the years with no VSCS are 24 for ARB which is 10 for BoB. In majority of the years, 1–2 TCs

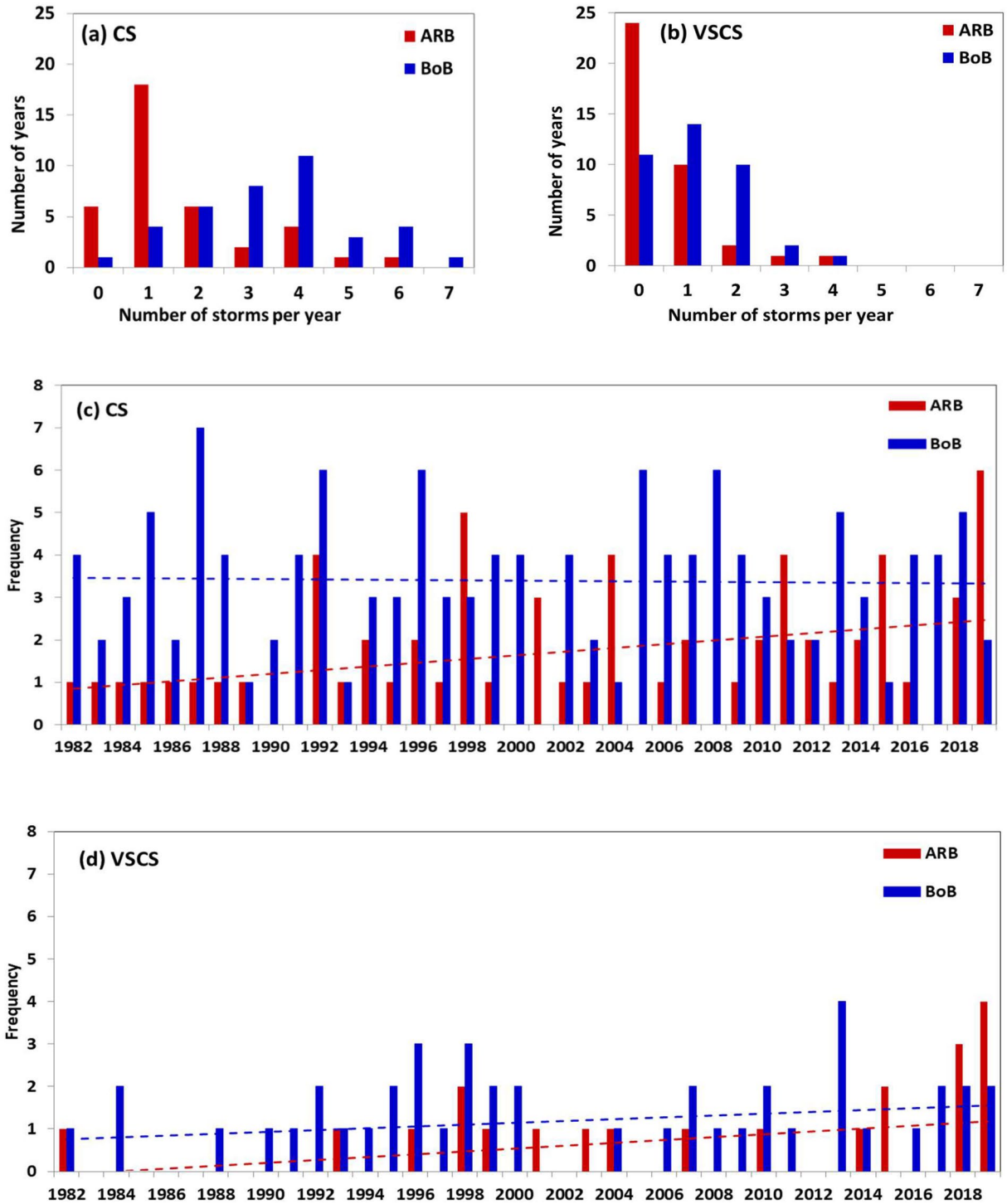

Fig. 1 Histogram of **a** CS, **b** VSCS category TCs. Time series (1982–2019) of TC frequency for **c** CS, **d** VSCS category TCs over the ARB (red bar) and the BoB (blue bar). Dash line shows the linear trend in TC frequency for the ARB and BoB

intensified to the VSCS category over BoB. There were eight typical years (1983, 1985, 1986, 1987, 1989, 2002, 2005 and 2012) when no TC reached VSCS strength in either of the basins.Time series and trends of TCs (CS and VSCS) annual frequency are shown (Fig. 1c, d). There is a significant increasing trend in ARB for both categories and no significant trend for BoB TCs. Hereafter, the word 'significant' is used when the p value is less than 0.05 from the regression analysis. For the majority of the years, the frequency of TC over the BoB is higher than that over the

Table 2 Frequency of CS and VSCS during PE and RE

Period	ARB	BoB	Total	Ratio BoB/ARB
PE 1982–2000	25 (6)	67 (23)	92 (29)	2.68 (3.83)
RE 2001–2019	38 (15)	62 (21)	100 (36)	1.63 (1.53)
Total	63 (21)	129 (44)	192 (65)	2.11 (2.19)
Ratio RE/PE	1.52 (2.5)	0.93 (0.91)	1.08 (1.24)	

The numbers in brackets indicate the frequency of VSCS

ARB except for 6 years (1998, 2001, 2004, 2011, 2015, and 2019) when the frequency of CS in the ARB is more than that in the BoB. Recently in 2015, 2018, and 2019, the frequency of TCs of VSCS category was also higher in the ARB than that in the BoB.

Further, we divide the 38 years into two epochs past epoch (PE) (1982–2000) and recent epoch (RE) (2001–2019) and presented TCs frequency in Table 2. The total number of TCs is 92 in PE and 100 in RE, out of this 30% intensified as VSCS in PE and 36% intensified in RE. More (less) number of TCs formed over ARB (BoB) in RE as compared with PE. During RE there is a 52% increase in CS frequency in ARB and an 8% decrease in BoB. For intense TCs (VSCS or above category) the increase in the frequency is twofold in ARB and no change in BoB. The last column of Table 2 is the ratio of BoB and ARB TC frequency. BoB is active compared to ARB but in RE this ratio has decreased. In RE, TC frequency has increased in the ARB and decreased slightly in the BoB.

The annual activity of TC in each basin is represented by the total duration (h) of TCs (CS and VSCS) which includes the effect of TC frequency and its lifespan. The trend in total duration of CS and VSCS per year is significantly increasing in the ARB (Fig. 2a, b), whereas, the trend in total duration of BoB CS and VSCS is insignificant. Similar to the frequency, in case of ARB, the total TC duration of CS category TCs has increased by 80% and about 3.5 times increase is seen for VSCS category duration in RE. However, for BoB the duration of CS and VSCS category TCs show no change in RE (Table 3).

This increase in the total duration of TC per year in ARB includes the effect of an increase in TC frequency. Hence, to single out the contribution from individual TC duration, a scatter plot of TC duration (Fig. 2c, d) for both the categories are shown. Results indicate a marginally significant ($0.05 < p$ value ≤ 0.1) increasing trend in the TC duration for ARB TCs, but no significant trends for BoB TCs. To compare each TC duration distribution in two epochs, the box and whisker plot is shown in Fig. 2e, f for CS and VSCS. It is based on the minimum and maximum values, the first (25th percentile) and third (75th percentile) quartiles and median (50th percentile) of the total distribution. The box represents the interquartile range which is the distance between the first and third quartile. In the plot, mean of the distribution is represented by a black diamond. Duration of CS category of TC's median (central line), interquartile ranges (boxes) and mean (black diamond) are the same but a decrease in minimum and maximum values of duration during recent years for BoB TCs is noted. For ARB, there is an increase in mean, median, interquartile ranges, and maximum value of CS category TCs. A similar pattern is seen for VSCS category TCs. So TC activity in terms of annual frequency and duration for CS and VSCS over ARB increased in recent years.

Now, to understand which months are contributing to these annual trends, the month-wise distribution of TC duration is plotted in Fig. 3a–d. Monthly climatology of CS category and VSCS category TC's duration is plotted for PE and RE in Fig. 3e, f. TCs are not there during January–April, July, and August in ARB except for a rare TC in 1983. Also when TC forms in May then in the same year no TC forms in June and vice versa (Evan and Camargo 2011). The first peak of ARB TC duration occurs during May–June and the second peak in October–November. BoB is active throughout the year except for February and August months. The first peak of BoB TC duration occurs during April–May and the second peak in November. In other months the CS category TCs duration is less but in general, there are active TC periods throughout the year in BoB. TC duration for CS in ARB is less compared to BoB but June is an exception when the ARB TC duration is more than TC duration in the BoB. Overall November is the most active month. Interestingly, CS and VSCS duration over ARB is higher (or approximately the same) during RE in all the active months. There were no VCSCs in PE in September–October but in the RE, VSCSs formed in these months. For BoB, in November the duration of CS and VSCS has reduced drastically in RE, whereas, a slight change is noticed in other months. There is an increase in TC (CS and VSCS) duration over ARB in recent years. An increase in CS duration is prominent in May and October. Regarding VSCS, an increase in duration is prominent in May, June, and October. For the BoB, the TC duration has reduced in November. The aforesaid months are discussed in Sect. 3.3. Based on monthly climatology of duration, pre-monsoon TC season is considered as April–June and post-monsoon season as October–December in this study.

To understand the relation of translational speed and TC duration, first translational speed of each TC is plotted against corresponding years (Fig. 4a, b). The corresponding trend and its significance is shown in Table 5. The scatter plot (Fig. 4a, b) shows a decreasing trend in the translation speed of TCs over ARB but the trend is not significant. A significant increasing (decreasing) trend is observed for BoB CSs during the pre (post) monsoon. Further to understand the distribution of translational speed in two epochs box

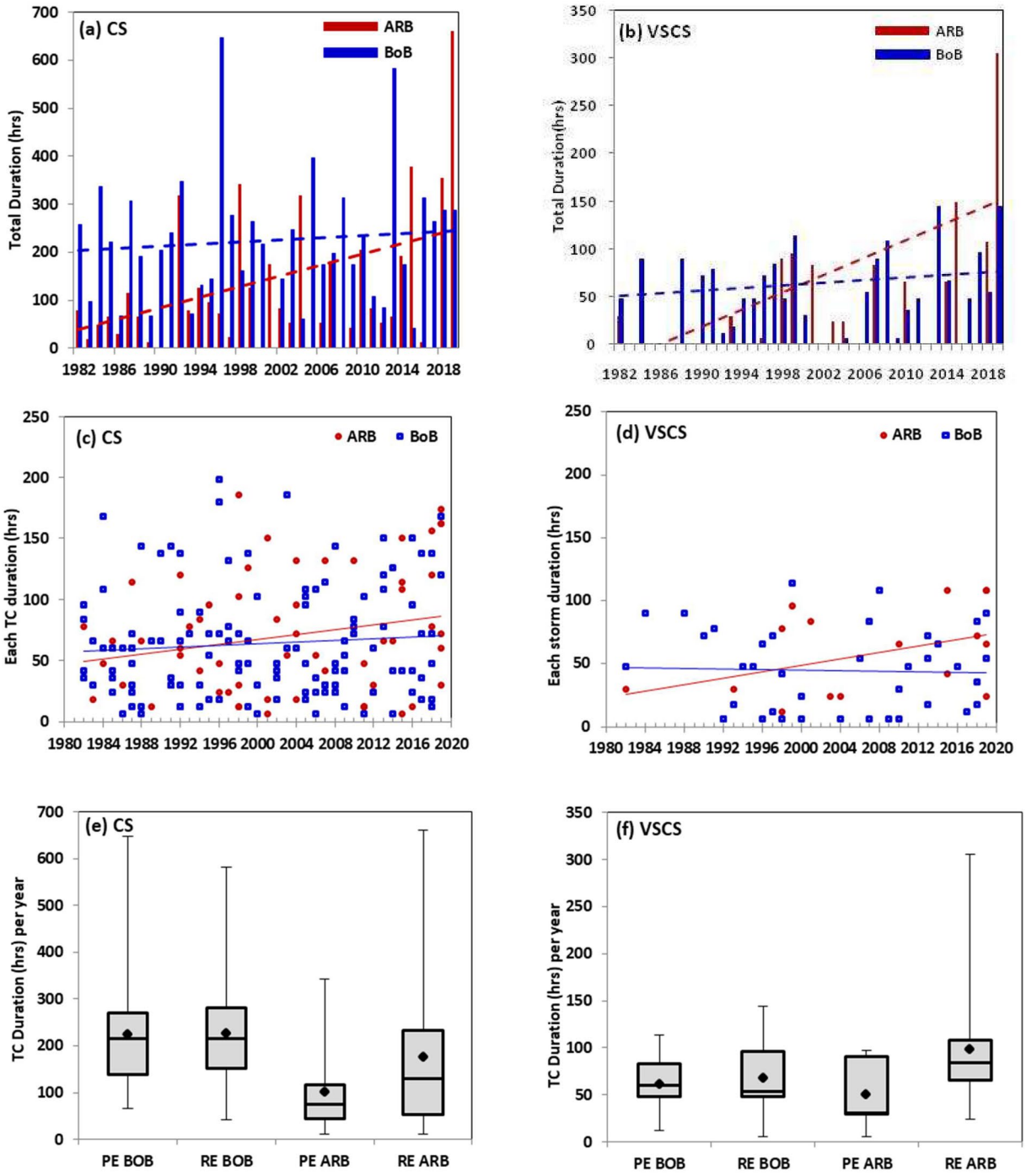

Fig. 2 Annual TC duration (h) for **a** CS, **b** VSCS category TCs in the ARB (red bar) and BoB (blue bar). Scatter plot of duration (h) per TC for **c** CS, **d** VSCS. Box and whisker plot for the distribution of total annual TC duration (h) during PE (1982–2000) and RE (2001–2019) in BoB and ARB for **e** CS and **f** VSCS

and whisker plot is presented in Fig. 4c, d. The decrease in translational speed is seen in RE for both the seasons for ARB TCs and post-monsoon BoB TCs, whereas an increase in translational speed is noted for BoB TCs during the pre-monsoon season. To quantify the relation of translational speed with the TC duration, correlation coefficients are provided in Table 6. The duration and translational speed of each TC are negatively correlated but the correlation is not significant except for the BoB pre-monsoon season. Our results are consistent with Kim et al. (2020) which shows that in the satellite era i.e. 1982 onwards there is a

Table 3 Total TC duration (h) CS and VSCS during PE and RE

Period	ARB	BoB	Total	Ratio BoB/ARB
PE 1982–2000	1614 (252)	4248 (852)	5862 (1104)	2.63 (3.38)
RE 2001–2019	2904 (912)	4080 (900)	6954 (1812)	1.40 (0.99)
Total	4518 (1164)	8328 (1752)	12,816 (2916)	1.84 (1.51)
Ratio RE/PE	1.80 (3.62)	0.96 (1.05)	1.19 (1.61)	

The numbers in brackets indicate the frequency of VSCS

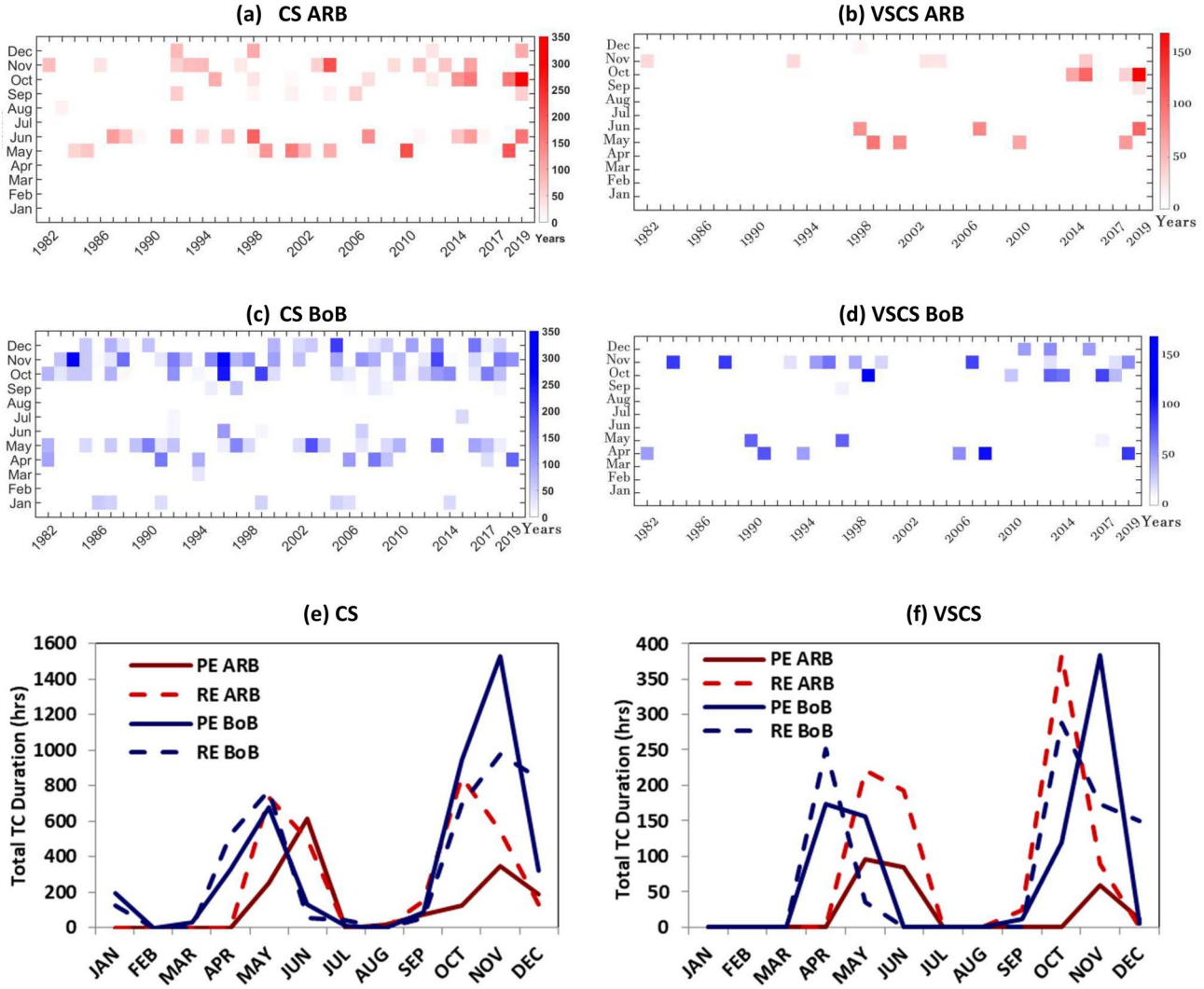

Fig. 3 Month-wise distribution of duration (h) for ARB **a** CS, **b** VSCS category TCs. **c**, **d** Same as **a**, **b** but for BoB. Month-wise distribution of total TC duration (h) during PE and RE for TCs of **e** CS, **f** VSCS

decreasing trend of translation speed over the north Indian Ocean cyclones.

To investigate the changes in the strength of TCs, ACE and lifetime maximum intensity (LMI) during pre-monsoon and post-monsoon season, an analysis of these parameters are presented (Fig. 5a–h). The significant increasing trend in LMI and ACE is noticeable for the ARB post-monsoon TCs, whereas, for BoB post-monsoon TCs, the increasing trend in ACE and LMI is marginally significant (Fig. 5a, b, e, f). This increase in LMI is in agreement with (Elsner et al. 2008). Regarding BoB TCs; mean, median and extreme values from box and whisker plots are the same for PE and RE but, the interquartile range has reduced in pre-monsoon season for BoB TCs in recent years. On the contrary, interquartile range

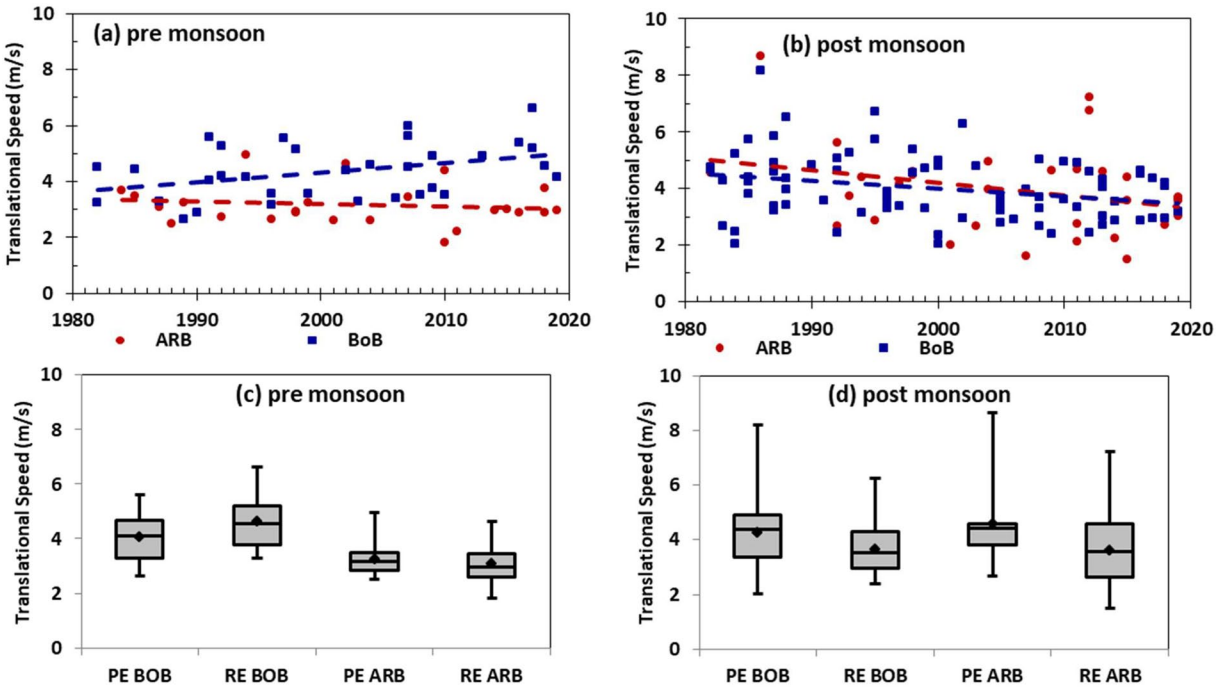

Fig. 4 **a**, **b** Scatter plot of translational speed (m s^{-1}) per TC for pre-monsoon and post-monsoon season. **c**, **d** Box and whisker plot for the translational speed for pre-monsoon and post-monsoon during PE (1982–2000) and RE (2001–2019) in BoB and ARB

Table 4 Total ACE (knot2) for ARB and BoB during PE and RE

Period	Pre monsoon	Post monsoon	Total	Ratio (BoB/ARB)
PE 1982–2000	45.57 (87.25)	27.28 (158.12)	72.85 (245.37)	3.3682
RE 2001–2019	93.44 (83.76)	114.16 (164.92)	207.6 (248.68)	1.1979
Ratio PE/RE	2.0505 (0.98)	4.1845 (1.0430)	2.8497 (1.0135)	

The numbers in brackets indicate the frequency of BoB

and maximum values of ACE and LMI in RE have increased for both seasons of ARB TCs. This indicates the increase in the spread of the ACE and LMI values and an increase in ACE and LMI maximum values over ARB.

Table 4 displays the total ACE for the two epochs. As expected, ACE is always higher for BoB than ARB, except in the pre-monsoon season during RE. Considering the pre-monsoon and post-monsoon together the ratio (BoB and ARB) of ACE was 3.36 in PE, which has become 1.21 in the RE. This indicates an increase in ACE in ARB basin in the RE. Ratios of RE to PE are calculated (Table 4 last row). In RE a fourfold (twofold) increase in ACE is seen for the post (pre) monsoon ARB TCs and there is no significant change for BoB. Considering the pre-monsoon and post-monsoon season together the ratio of the RE and PE is 2.72 for ARB and 0.98 for BoB.

A difference in the spatial distribution of ACE over ARB in both seasons (Fig. 6) is noticed with an increase in ACE during the RE. In PE over ARB, ACE is north–south aligned as the majority of the intense TCs are tracking towards the north direction. In RE along with north–south orientation, ACE covers almost the entire ARB. No TC crossed the Gulf of Oman in PE. However, in the RE during the pre-monsoon season, intense TCs are tracking towards this region. This is in agreement with Wang and Toumi (2021) which shows that there is a westward shift in the cyclone track in the north Indian Ocean. However, in the BoB, not much change in the magnitude and distribution of ACE is observed, but in the pre-monsoon season, the ACE has decreased in RE compared to PE.

3.2 Environmental conditions favourable for TC genesis and intensification

The previous section substantiates that the number of TCs per year, and intensity of TCs are changing over NIO, particularly in the ARB. The number, duration, LMI, and ACE of TCs are significantly increasing in the ARB. This is in agreement with previous studies (Evan et al. 2011; Wang et al. 2012; Murakami et al. 2017). The prominent change is

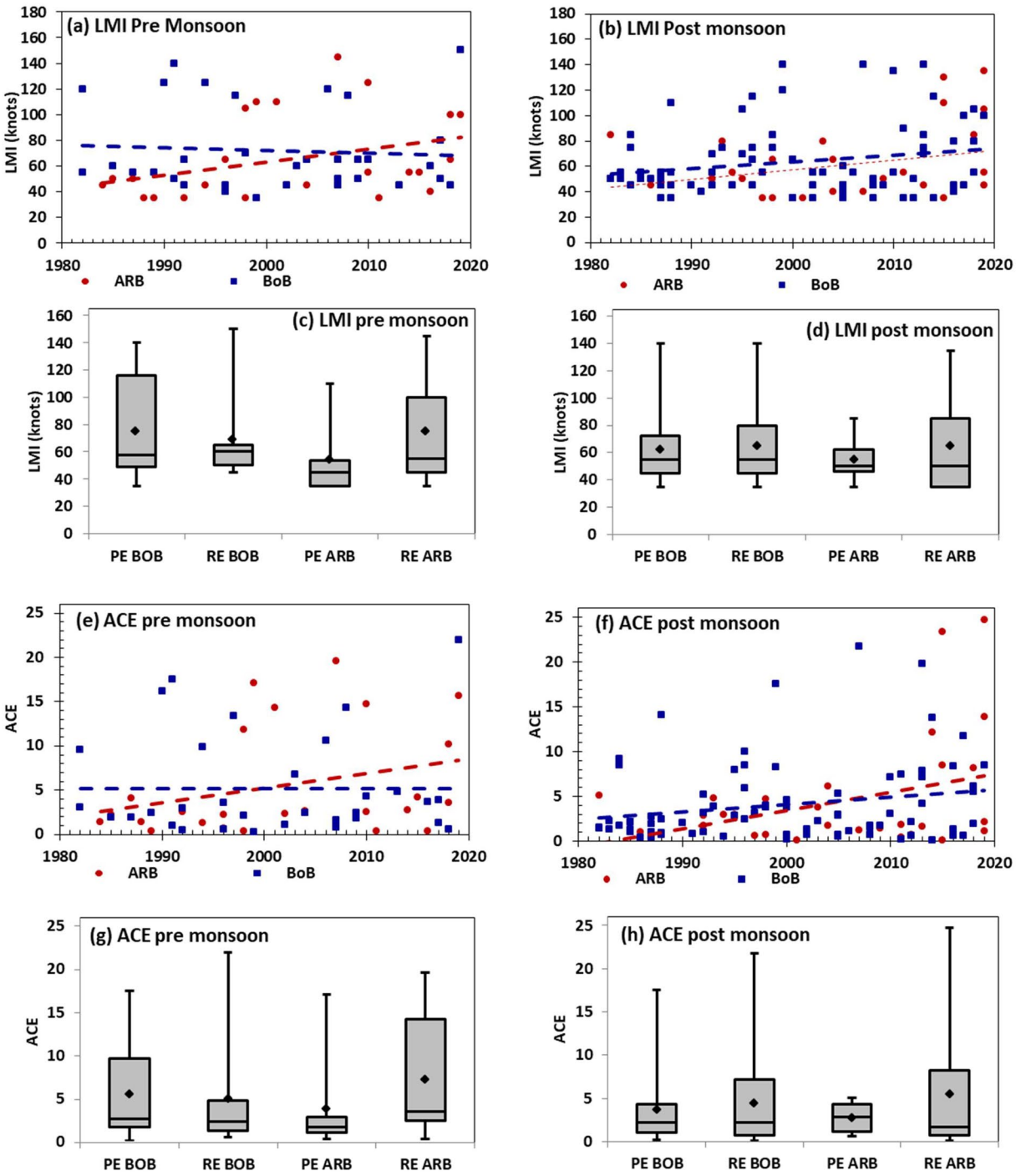

Fig. 5 Scatter plot of lifetime maximum intensity (LMI) (knot) per TC for **a** pre-monsoon, **b** post-monsoon. Box and whisker plot for LMI (knot) during PE (1982–2000) and RE (2001–2019) over BoB and ARB for **c** pre monsoon and **d** post monsoon. **e**–**h** Same as **a**–**d** but for ACE (knot^2)

seen in May, June, October and December. The TC genesis and intensification are governed by various dynamical and thermodynamical parameters such as SST, mid-level relative humidity, moist static energy, low-level vorticity, vertical wind shear, etc. GPI includes these parameters (Suneeta and Sadhuram 2018) and indicates the favourable environment for TC genesis. Figure 7a and b shows the spatial trend in GPI during the pre-monsoon and post-monsoon seasons. During pre-monsoon, GPI is increasing over parts of central ARB and near Somalia coast but decreasing near Oman

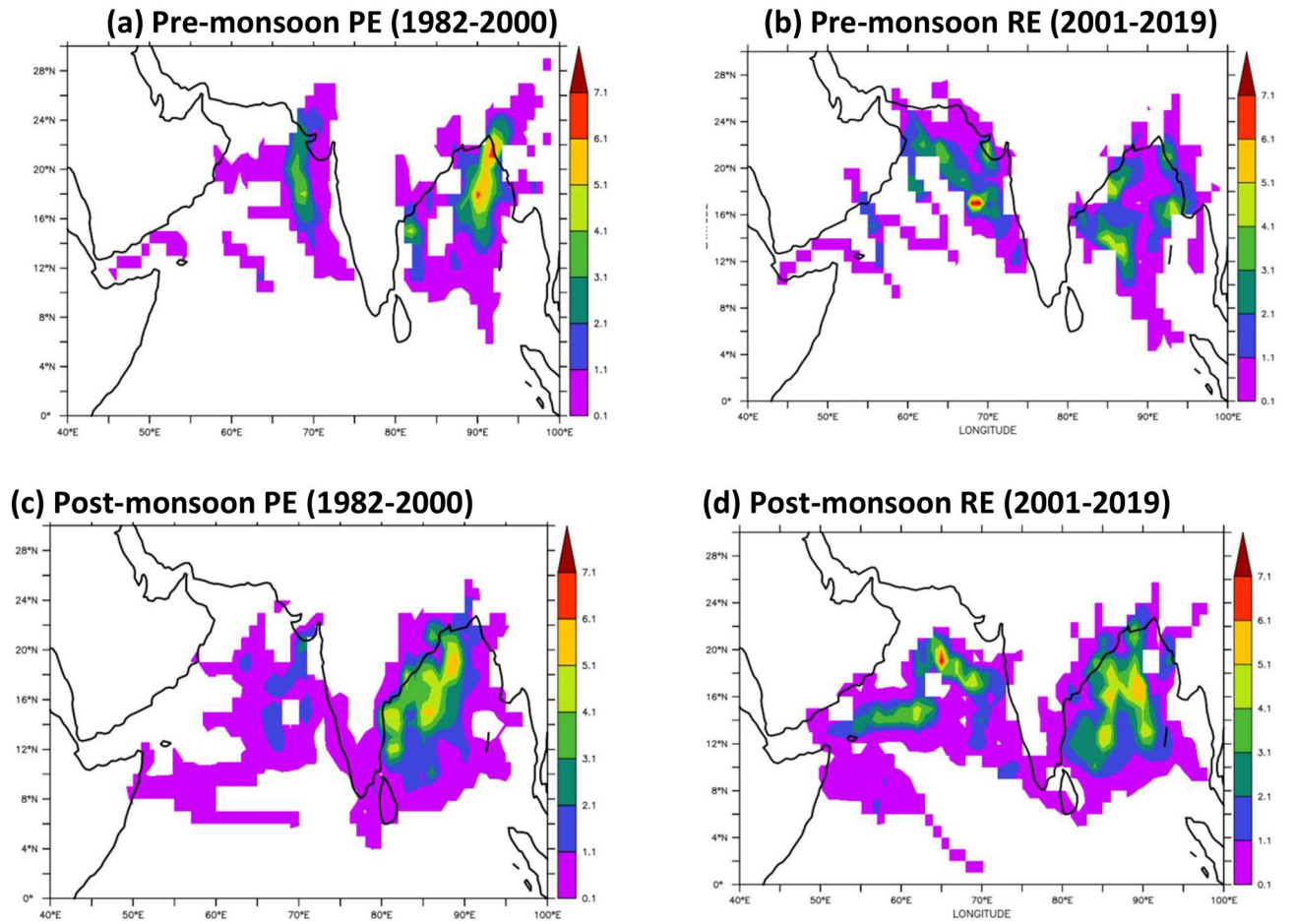

Fig. 6 ACE (knot^2) over north Indian ocean for pre-monsoon **a** PE (1982–2000), **b** RE (2001–2019), **c**, **d** same as **a**, **b** but for post-monsoon

and Yemen. Over the east BoB a decreasing trend and over west BoB an increasing trend in GPI is noted. During the post-monsoon season, a significant increasing trend over the east ARB and decreasing trend over the west BoB are observed. Along with GPI, potential intensity (PI) in terms of maximum wind speed (m s^{-1}) is calculated, which is the TCs intensity estimation based on thermodynamic state of the atmosphere and the sea surface (Bister and Emanuel 2002). The spatial trend in PI (Fig. 7c, d) indicates a significant increasing trend over ARB and BoB. During the pre-monsoon season, trend in PI is not significant over both the basins except an increasing trend over the Persian Gulf and a decreasing trend near Somalia.

GPI and PI show the combined effect of various parameters, to understand the contribution of individual parameters in the changes observed in the cyclogenesis and its intensification; first, we analysed the spatial trend in TCHP and SST for 38 years (Fig. 7e–h). TCHP is an estimation of ocean heat content available for cyclone–ocean interaction. Sharma and Ali (2014) showed that ocean heat content plays an important role in governing the life cycle and intensity of cyclones in the north Indian Ocean. High ocean heat content implies a warmer upper ocean, which provides a large amount of uninterrupted supply of sensible and latent heat fluxes from the ocean surface to the atmosphere that helps the cyclone to intensify (Shay et al. 2000). It is very interesting to note that during the pre-monsoon season, though SST shows a significant increasing trend over the entire ARB and north-east part of BoB, TCHP is increasing only over the Indian coast of ARB and part of east and central BoB. This is the region where ACE has also increased in RE but over remaining BoB ACE has decreased. Further, during the post-monsoon season SST is increasing significantly throughout the BoB and the ARB. This rapid warming of the entire north Indian Ocean is in agreement with Roxy et al. (2019). But TCHP is increasing only along the Indian coastline of BoB. This basin-wide warming of the north Indian Ocean provides conducive conditions for the rapid intensification of TCs provided atmospheric conditions remain favorable. Consistent with the increasing trend in TCHP, there is an increasing trend in SST over both the basins, except for decreasing trend

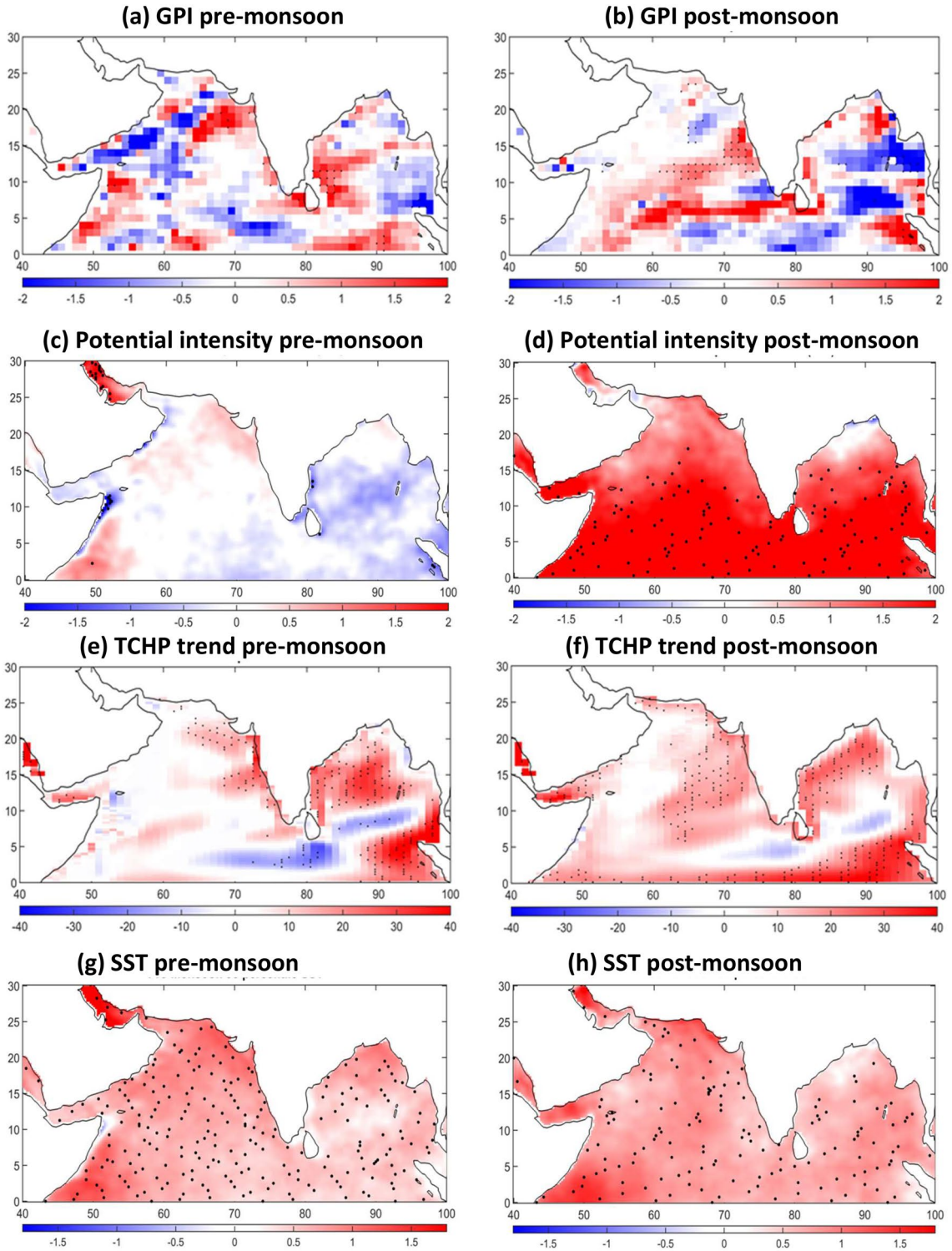

Fig. 7 Total trends in **a**, **b** Genesis Potential Index (GPI), **c**, **d** potential intensity (m s^{-1}), **e**, **f** TCHP (J m^{-2}) and **g**, **h** SST (°C) for pre-monsoon and post-monsoon during 1982–2019. Dots over the color denote the regions where the total trend in SST and TCHP is significant at 95% confidence level

near the Somalia coast during the pre-monsoon. The highest increasing trends are observed during the pre-monsoon season in the Persian Gulf. A significant trend is seen in the north ARB and the west equatorial Indian ocean. This overall increase in TCHP and SST enhances the chances of cyclogenesis and intensification, and hence could be

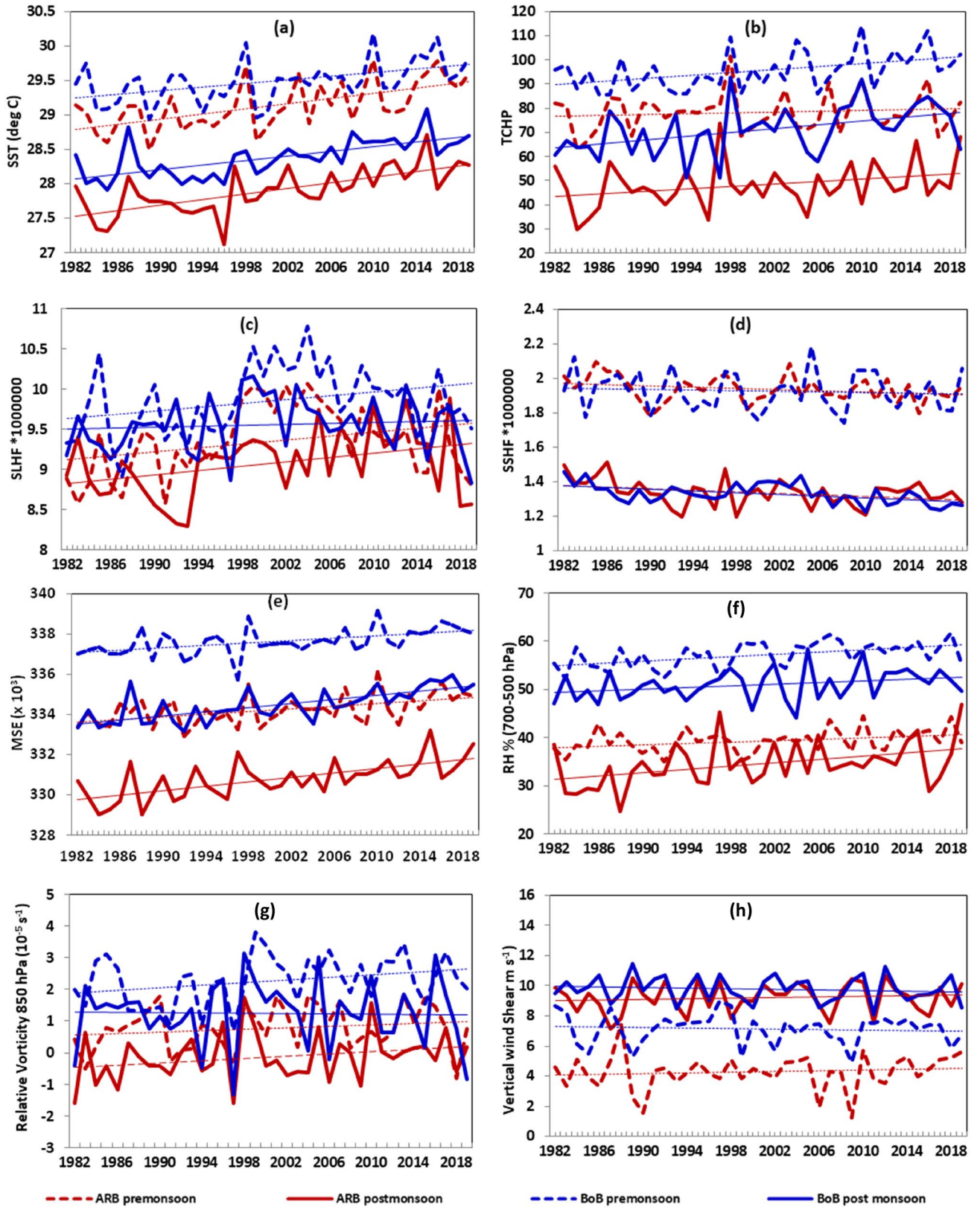

Fig. 8 Time series trend analysis for **a** SST (°C), **b** TCHP (J m^{-2}), **c** SLHF (J m^{-2}), **d** SSHF (J m^{-2}), **e** column (950-150 hPa) averaged MSE (J kg^{-1}), **f** mid-level RH (%), **g** 850 hPa relative vorticity (10^{-5} s^{-1}) and **h** vertical wind shear of horizontal wind (m s^{-1})

Table 5 Total trend for 1982–2019 (38 years) and p value from regression analysis for various parameters related to TC activity over BoB (blue) and ARB (red)

	Trend	P value	Trend	P value
	CS		VSCS	
Frequency	**1.67**	**0.04**	**1.28**	**0.01**
	-0.14	0.88	0.81	0.15
Duration of each TC (hrs)	38.15	0.08	48.15	0.08
	12.62	0.37	-4.08	0.83
Total Active Duration (hrs) per year	**214.76**	**0.01**	**172.54**	**0.02**
	42.15	0.57	25.62	0.33
	Pre monsoon (April-May-June)		Post monsoon (Oct-Nov-Dec)	
Duration (each TC)	35.23	0.32	34.32	0.27
	13.26	0.66	20.97	0.22
Translational Speed (m s^{-1}, each TC)	-0.35	0.49	-1.69	0.11
	1.27	**0.03**	**-1.04**	**0.01**
ACE (each TC) (knots^2)	6.32	0.14	**7.77**	**0.05**
	-0.05	0.99	3.14	0.06
LMI (each TC) (knots)	**38.70**	**0.09**	**28.62**	**0.15**
	-7.99	**0.70**	**19.82**	**0.06**
Potential Intensity (PI)	0.06	0.88	**1.64**	**0.00**
	-0.31	0.51	**1.49**	**0.00**
Sea Surface Temperature (°C)	**0.72**	**0.00**	**0.77**	**0.00**
	0.50	**0.00**	**0.64**	**0.00**
Tropical Cyclone Heat Potential (kJ/cm^2)	2.93	0.51	9.44	0.07
	12.14	**0.00**	**15.18**	**0.00**
Surface Latent Heat Flux (J/m^2)	**464291**	**0.05**	**512953**	**0.02**
	448093	0.06	106672	0.58
Surface Sensible Heat Flux (J/m^2)	-70733.87	0.08	**-87076.89**	**0.04**
	-34632.56	0.58	**-98894.53**	**0.00**
Moist Static Energy (10^3 J/kg) (950-150 hPa)	**1.23**	**0.001**	**2.09**	**0.00**
	1.13	**0.001**	**1.96**	**0.00**
Mid (700-500) Level Relative Humidity (%)	**2.85**	**0.03**	**6.47**	**0.01**
	4.61	**0.00**	**3.37**	**0.05**
850 hPaRelative Vorticity (10^{-5} s^{-1})	0.44	0.26	0.65	0.13
	-0.08	0.89	0.79	0.06
Vertical wind shear of horizontal wind(m s^{-1})	0.48	0.47	0.40	0.47
	-0.3	0.59	-0.41	0.39

*$p > 0.1$ not significant, $0.05 < p < 0.1$ marginally significant, $p < 0.05$ significant and $p < 0.01$ highly significant

responsible for higher ACE in east ARB during the pre-monsoon season.

Figure 8 displays the time series trend analysis of environmental parameters favourable for TC genesis and intensification. Trend magnitude along with trend analysis confidence level is shown in Table 5. The increasing trend in SST for both seasons and basins is significant. TCHP is increasing significantly in BoB but the trend of TCHP in ARB is not significant in both seasons. TCs extract latent heat energy from the underlying warmer ocean. The latent heat flux plays a crucial role in cyclogenesis and intensification (Grodsky et al. 2009). The magnitude of surface latent heat flux (SLHF) in Fig. 8c indicates an increasing trend implying an increased heat transfer from the ocean to

the atmosphere. Here the positive values indicate upward fluxes meaning heat transfer from the ocean to the atmosphere which is favourable for cyclogenesis and its intensification. The trend in ARB is significant for both seasons. The significant decreasing trend in surface sensible heat flux (SSHF) over ARB and BoB is noted in the post-monsoon season (Fig. 8d). Moist static energy and mid-level relative humidity (Fig. 8e, f) are increasing significantly over ARB, consistent with an increase in TCHP and SST. The relative humidity plot is showing an increasing trend in the pre-monsoon and post-monsoon season, on the other hand, moist static energy is showing an increasing trend only in the post-monsoon season. Since, moist static energy comprises internal energy, latent energy and potential energy, hence it shows the total energy acquired from the ocean. Further, we see that there is no significant trend in the dynamical parameters like 850 hPa relative vorticity and vertical wind shear in both the basins and both the seasons (Fig. 8g, h).

The increase in SST and TCHP increases the evaporation and thus there is an increase in the surface latent heat flux (ocean to the atmosphere). Surface latent heat flux is a function of Δq (i.e.q_s–q_a) and wind speed, where q_s and q_a are surface saturated and near-surface air specific humidity respectively. To check the role of winds in increasing evaporation we analysed surface wind speed (10 m) obtained from ERA5 for the study period (figure not shown). There is no trend in surface wind speed during 38 years for both the basins and seasons indicating surface wind speed have not changed over the period. In general increase in SST and TCHP increases q_s and q_a. For the north Indian ocean, Bhat (2003) shown that Δq follows SST very closely in the Bay of Bengal/Indian Ocean but q_a is not well coupled with SST (Joseph et al. 2017) over parts of equatorial Indian ocean. All these indicate increasing SST and TCHP increases qs and thus surface latent flux and evaporation. Warmer SST enhances surface flux and RH in the boundary layer but, there are complexities involved in understanding the pathway of surface fluxes to the RH in the free troposphere. One of the mechanisms which pump the RH in the boundary layer to the middle-higher troposphere is the deep convection. To evaluate the space-time behaviour of deep convection one of the way is to analyse satellite measurements of OLR (Ohring and Gruber 1983). We plotted spatial trend in OLR (Fig. 9) which shows a significant decreasing trend over ARB and BoB during both the seasons. Decreasing OLR indicates an increasing trend in deep convection. Recently Zhang et al. (2017) concluded that enhanced deep convection (lower OLR) is linked to amplified heating in the tropical troposphere based on correlation patterns and composite analyses. Deep convection is the precursor for the genesis and intensification of TCs.

In general, the thermodynamic environmental conditions, particularly the SST, TCHP, SLHF, MSE, and RH are becoming favourable over both the basins in recent years. The correlation of these parameters with the duration of the TC for CS category and with each other is presented in Table 6. Correlation of ACE with duration is significantly high ($CC > 0.5$) for TCs over ARB during both the seasons and BoB during the pre-monsoon season. CS total duration per year is positively correlated with MSE for TCs over ARB in both seasons. RH also positively correlated with TC duration over ARB in the post-monsoon season. Correlation is not significant with either of the parameter over BoB. Positive correlations of MSE with SST and TCHP, indicate an indirect role of SST and TCHP in increasing TC duration. The correlation is higher for ARB pre-monsoon, ARB post-monsoon, and BoB post-monsoon seasons but weaker for the BoB pre-monsoon season. So, particularly an increase in column averaged (950-150 hPa) MSE is playing a dominant role in the observed increase in TC frequency in ARB. This increase in MSE is due to an increase in SST in ARB.

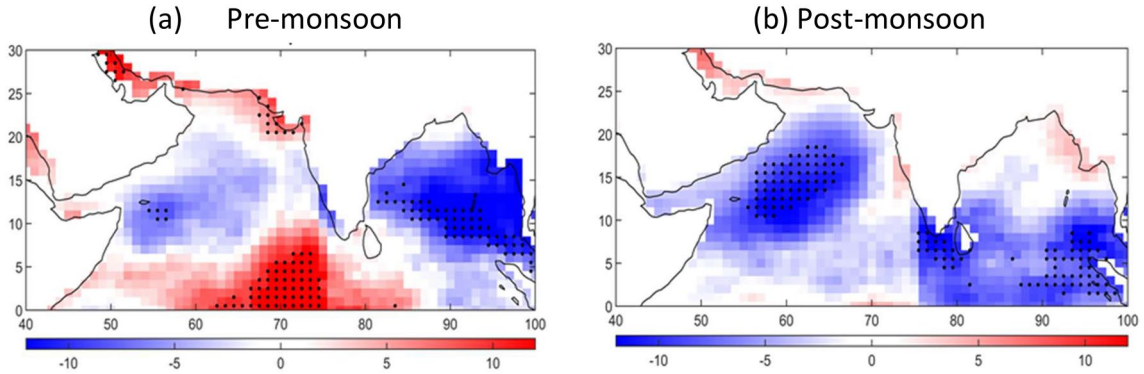

Fig. 9 Trend in OLR (W m^{-2}, shaded) during the period 1982–2019 for **a** pre-monsoon, **b** post-monsoon. Dots over the color denote the area where the trend is significant at 95% confidence level

Table 6 Correlation coefficients (CC) of various parameters (Bold CCs are significant at 95% confidence level)

	ARB pre monsoon	ARB post monsoon	BoB premonsoon	BoB post monsoon
DUR (each TC) and TR SPEED	− 0.02	− 0.09	**− 0.37**	− 0.17
ACE DUR	**0.63**	**0.72**	**0.65**	0.3
ACE PI	0.23	0.16	0.01	0.1
ACE and MSE 950-150	0.23	**0.68**	0.11	0.13
ACE SST	0.23	**0.49**	0.04	− 0.02
ACE RH	0.11	**0.54**	− 0.1	0.18
ACE TCHP	0.18	0.31	− 0.05	0.1
DUR and PI	0.16	0.18	0.01	0.12
DUR and MSE 950-150	**0.43**	**0.59**	0.12	0.08
DUR and SST	**0.45**	0.31	0.14	− 0.14
DUR and RH	0.26	**0.6**	− 0.23	0.22
DUR and TCHP	0.41	0.36	0.02	0.14
SST and PI	**0.45**	**0.49**	0.24	**0.55**
SST and MSE 950-150	**0.91**	**0.78**	**0.60**	**0.74**
TCHP and PI	**0.59**	0.34	0.17	0.2
TCHP and MSE 950-150	**0.81**	**0.74**	**0.65**	**0.62**
SST and RH	**0.61**	**0.54**	− 0.06	0.34
TCHP and RH	**0.48**	**0.78**	0.13	**0.34**
PI and RH	0.12	0.14	0.09	0.25
MSE 950-150 and RH	**0.78**	**0.82**	**0.52**	**0.68**

DUR (each TC): duration of each TC, TR SPEED: translational speed of each TC, ACE: average ACE per year, DUR: total duration per year

3.3 Tracks, genesis, and intensification locations

Figure 10 shows genesis locations and tracks of TCs in two epochs and two seasons. Comparing PE and RE (Fig. 10a, b) there is not much change in the distribution of genesis location of TCs in BoB, but, a significant change is seen in ARB during the post-monsoon season (black circles). In PE there were three TCs within the lower (0°–8° N) latitudes; however, in RE ten TCs has genesis in this region. The majority of the TCs forming in latitudes greater than 10° N are in the post-monsoon season. Also, it is observed that no TC has formed in the west equatorial ARB (0°–8° N, 50°–67° E) in the PE compared to RE. In the west-central ARB, the number of TCs is the same in PE and RE but TCs are distributed at lower latitudes in RE. In the east-central ARB (> 8° N and > 67° E), more TCs are forming in the post-monsoon season in RE. TCs are aligned close to the west coast of India in PE. SST is warmer in RE throughout the NIO (Fig. 7) thus favorable for genesis and intensification of TCs. The increase in TCHP at lower latitudes particularly over the south-central ARB is responsible for genesis at lower latitudes along with other favorable atmospheric conditions. This shift in the genesis location equatorward is in agreement with Daloz and Camargo (2018) which show that during the period 1980–2013, an average equatorward shift of genesis location for the north Indian Ocean TCs is 78 km decade^{-1}.

The changes in genesis locations are prominent during May, June, October and November. Also in the previous section (Fig. 3e, f) we discussed that changes in TC activity are observed during these four months. Thus to understand the causes for these changes, the difference (RE–PE) in mid-level (700–500 hPa) RH and vertical wind shear of horizontal wind (levels 850 hPa and 200 hPa) are shown (Fig. 11a–d) for May, June, October and November. An increase in mid-level RH between 8 °N and 16° N in May and over the north ARB in June is observed which may be providing a favorable environment along with higher SST and TCHP. Thus there is an increase in the duration of CS and VSCS category TCs in ARB during May and June (Fig. 3e, f). Strikingly there is an increase in mid-level RH over the entire ARB during October–November with a prominent increase in lower latitudes (0°–10° N). This is the region where the genesis of TCs has increased in RE during the post-monsoon. As the genesis of TCs is at lower latitudes, the duration of TCs has also increased. With increasing SST, and mid-level RH the

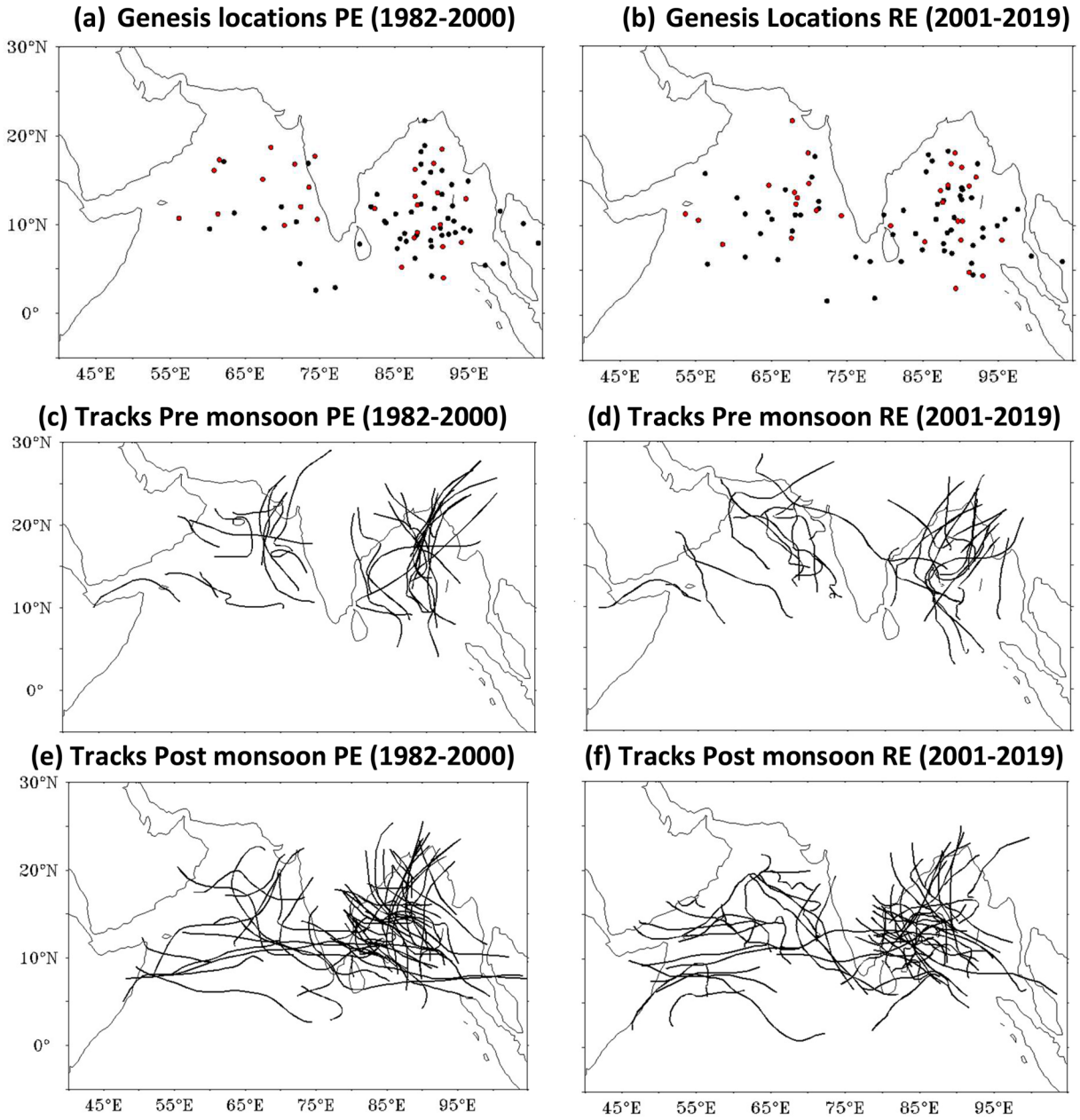

Fig. 10 TC Genesis locations (solid circles) for pre-monsoon (red) and post-monsoon (black) during **a** PE (1982–2000), **b** RE (2001–2019). Tracks of TCs for pre-monsoon **c** PE (1982–2000), **d** RE (2001–2019), **e**, **f** same as **c**, **d** but for post-monsoon season

boundary layer becomes more humidified resulting in the cyclones maintaining their intensity or even intensify further (Rappin et al. 2010). Thus, there is a maximum increase in the duration of CS category TCs in October and November. On the contrary, there is a decrease in mid-level humidity over BoB in November, and the duration of CS and VSCS category TCs also show a decrease in RE (Fig. 3e, f).

Regarding tracks (Fig. 10c–f), there are three categories of tracks in general; westward, north-westward and northward. Few TCs recurve with initial north-westward movement and then turning to north-east or east. During the post-monsoon, tracks of TCs over both basins are almost the same in two epochs but the change in TC tracks is seen in the pre-monsoon. In the pre-monsoon PE, TCs in BoB are moving north-westward and crossing the east coast of India. However, in RE few TCs are crossing the east Indian coast. The majority of TCs are moving northward or recurving towards the east and north-east. The change observed in the tracks over ARB near the Oman coast is due to tracks in the pre-monsoon season. There is a slight change in the track locations, particularly over the region north of 20° N and

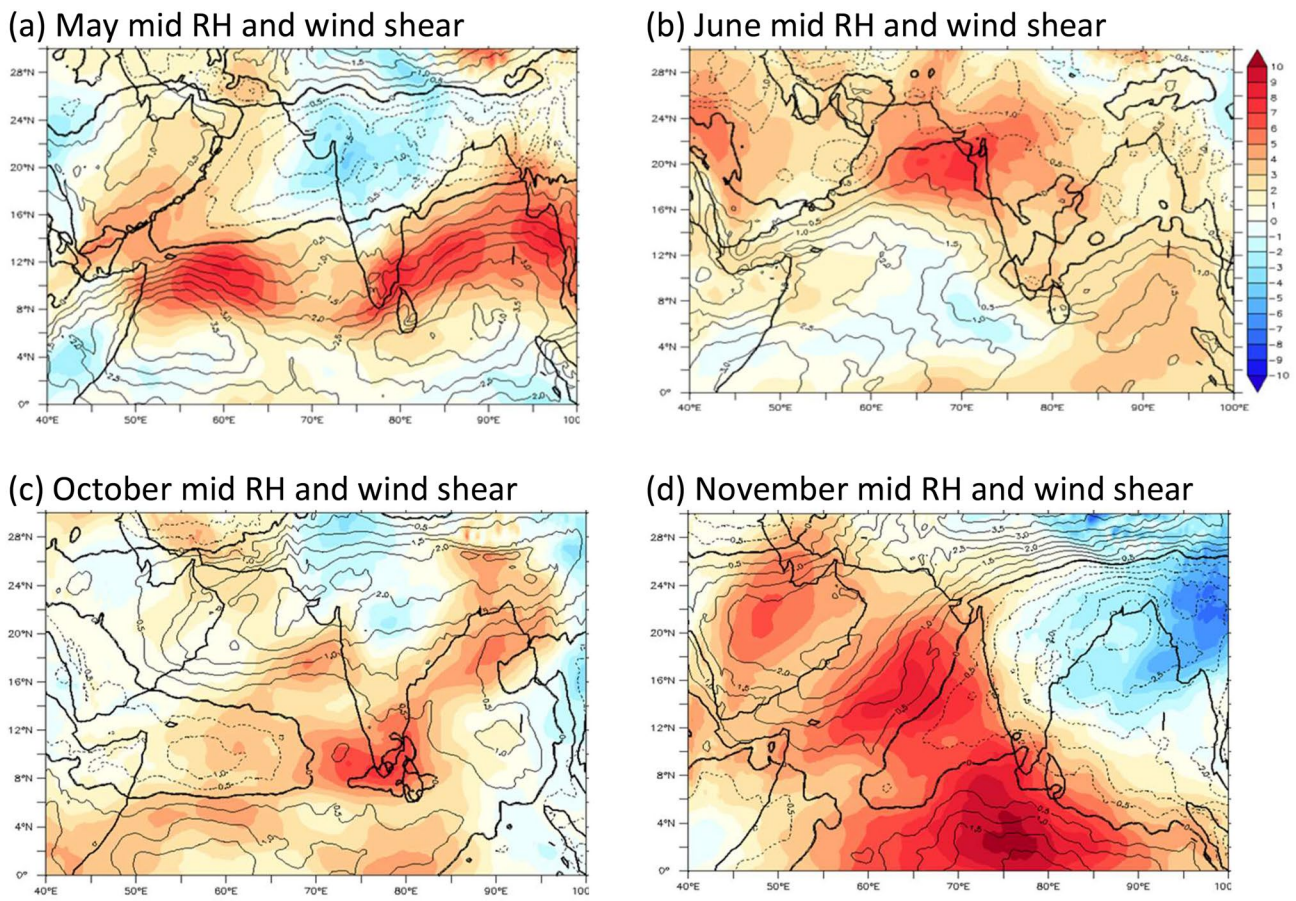

Fig. 11 Relative humidity difference (RE–PE) (%, shaded), vertical wind shear difference (RE–PE) (m s^{-1}, contours with the interval of 0.5) for the month of **a** May, **b** June, **c** October and **d** November

west of 65° E in the ARB. The majority of the TCs reaching this area during the RE are formed in June. Noting these changes in the tracks, the steering wind (700–200 hPa average) is plotted (Fig. 12) for the duration of the storms. The steering current is plotted separately for the TCs in the two basins. Here the vortex is removed before averaging the wind to exclude the impact of the TC on the steering.

In April for BoB TCs, anticyclone (marked A in the figure) near the Myanmar coast is steering the tracks so TCs are moving northward along the western periphery of anticyclone (Fig. 12a, b). In RE, the anticyclone has shifted slightly southward so TCs are recurving eastwards and are making landfall near Yangon which was not seen in the PE. The month of May is active for both the basins and again ridge (anticyclone) over Myanmar is steering the TCs in the BoB (Fig. 12c, d). In RE, there is anticyclone over ARB extended up to the Indian landmass which is the reason TCs are moving along the east coast and not crossing the Indian coast during RE. For TCs in ARB during May (Fig. 12e, f), anticyclone over central India is steering the TCs, so TCs were moving northward in the PE. This anticyclone is elongated and covering the ARB so the tracks are also westward in the RE. The case of TC Phet, 2010 is perfectly explained by this steering. In June (Fig. 12g, h), TCs in the ARB are crossing north Oman and entering into the Gulf of Iran in RE due to the weakening of anticyclone over that region. In PE, this region was avoided due to the presence of anticyclone. BoB October TCs are steered by a ridge to the east over Myanmar (figure not shown). There is no change in steering but less number of TCs in RE. For ARB TCs in October (Fig. 12i, j), there are two steering anticyclones (one over Arabia and another over Myanmar extended till the Indian peninsula. In RE these anticyclones have shifted slightly southward. As the genesis of the TC is also more in lower latitudes, so the tracks of the TCs are westward due to strong easterlies crossing Yemen and Somalia. In general the changes in steering currents responsible for changes in the tracks are noted in this study. These need to be explored in future studies to understand the reasons for the existence of such circulation patterns.

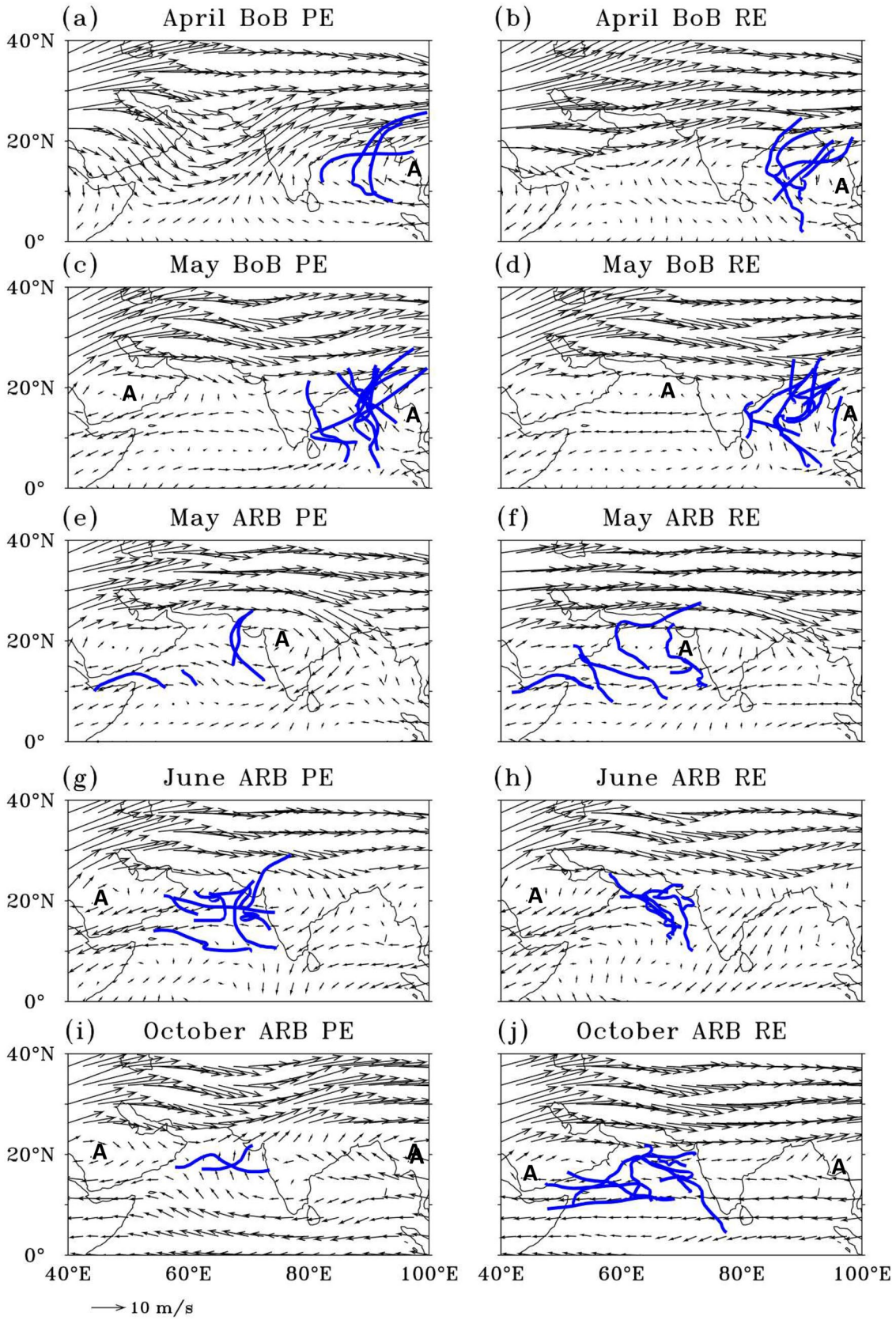

Fig. 12 Steering currents (wind m s^{-1} averaged over 700–200 levels) for **a**, **b** April BoB TCs, **c**, **d** May BoB TCs, **e**, **f** May ARB TCs, **g**, **h** June ARB TCs and **i**, **j** October ARB TCs for PE (1982–2000) and RE (2001–2019)

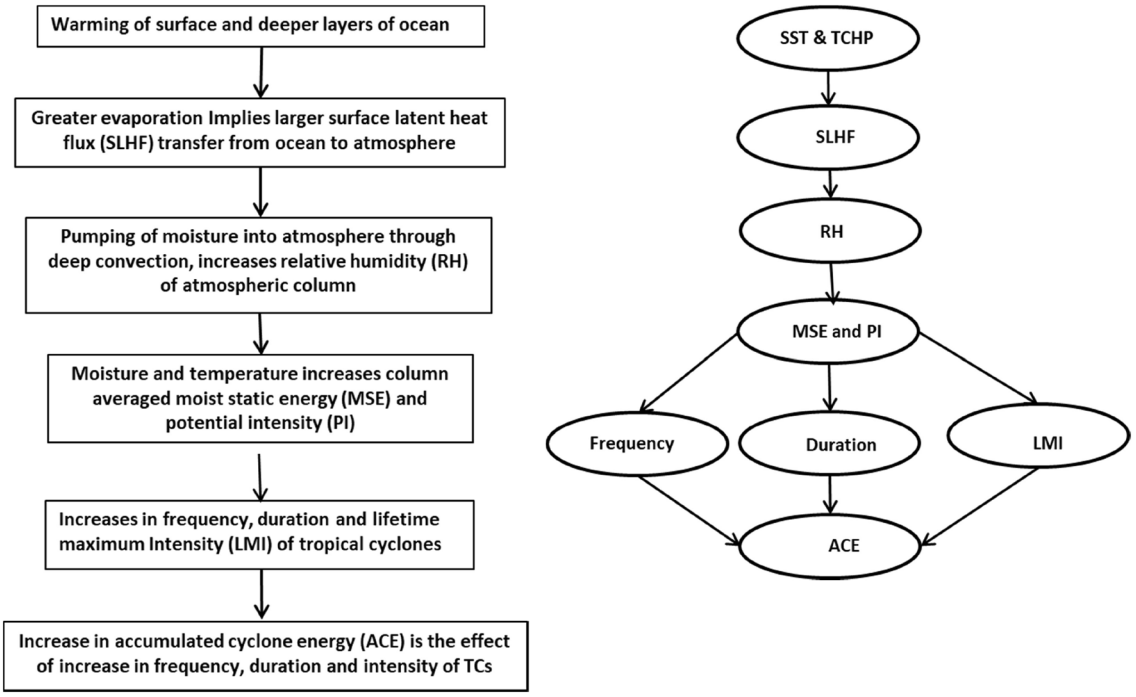

Fig. 13 Plausible mechanism for enhanced frequency, duration and lifetime maximum intensity of the TCs implying increased accumulated cyclone energy (ACE) over the Arabian Sea

4 Conclusions

Recent tropical cyclone (TC) activity over the north Indian ocean (NIO) raised the question—has TC activity over NIO changed with the changing climate? To understand this, we studied the trends in the frequency, duration, intensity, and favorable environmental parameters associated with TCs. For the period 1982–2019, we analyzed the TC activity of Arabian Sea (ARB) and Bay of Bengal (BoB) basins separately. TC activity in the BoB is generally higher than that of ARB. The ratio of frequency (BoB/ARB) was 2.7 in the past epoch (1982–2000) which is 1.6 for the recent epoch 2001–2019. In the Arabian Sea, increase in the frequency of TC is about 52% and the increase in the duration of TC is about 80%. On the other hand, there is almost no change in the frequency and duration of TC in the BoB. Also, the frequency and duration of intense TCs (VSCS) have increased in the recent epoch. Due to an increase in the frequency, intensity, and duration of TCs, Accumulated Cyclone Energy (ACE) has also increased in the recent epoch. The increase in ACE is twofold in the pre-monsoon (April–May–June) season and fourfold in the post-monsoon (October–November–December) season for the ARB TCs; however, no change in ACE is observed for the BoB TCs. During the study period, a significant increasing trend is seen in the total active duration of TC in ARB. Also for ARB, there is an increasing trend in ACE, SST, SLHF (ocean to atmosphere) for the post-monsoon season, and MSE, RH for both seasons.

The month-wise distributions of TC duration over ARB in the two epochs indicate a remarkable increase during recent epoch for May, June, and October. An increase in mid-level RH within 8° N–16° N in May and over the north ARB in June is providing a favorable environment along with higher SST and TCHP. The plausible mechanism for an increase in TC activity over ARB is presented (Fig. 13). The increase in SST and TCHP increases the evaporation and thus there is an increase in surface latent heat flux (ocean to the atmosphere). Further increase in the detrainment by deep convection is also observed. In effect, the mid-level RH and MSE over the column (950-150 hPa) increases which are correlated with the duration of the TCs. Strikingly, there is an increase in the mid-level RH over the entire ARB during October–November and the maximum increase is observed close to the equator (0°–10° N). This is the region where the genesis of the TCs is happening in RE. The genesis location at lower latitudes increases the duration of TCs with a longer track. Thus, there is a maximum increase in the duration of CS category TCs in October–November. On the contrary, a decrease in mid-level RH seems to be responsible for the reduction in duration of BoB TC in November. Duration of CS and VSCS also shows a decrease in the recent epoch. No specific change in genesis location is noted for the BoB TCs.

TCHP is significantly increasing along the Indian coastline over BoB, especially in the post-monsoon season, providing rapid intensification of TCs.

Regarding tracks, there are three categories of tracks in general; westward, north-westward and northward. Very few TCs are re-curving with initial north-westward movement and then turning to northeast or east. During the post-monsoon season, TC tracks appear to be same for ARB and BoB in two epochs but change is visible for pre-monsoon TCs over both the basins. In the past epoch, some of the BoB TCs are moving northwestward and crossing the east coast of India. However, in the recent epoch, very few TCs are crossing the east Indian coast, the majority are moving northward or recurving towards east. There is a slight change in tracks, particularly over the region north of 20° N and west of 65° E over the ARB. In May during past epoch the ARB TCs are steered northward by an anticyclone present over central India landmass. Whereas in recent epoch this anticyclone is elongated, thus steers the TCs toward the west. There is an anticyclone over Arabian Peninsula in June that is slightly elongated, which is the reason tracks are along the east coast and not crossing the Indian landmass during the recent epoch. The reasons for these changes in circulation patterns need be explored in future studies. In general, the TCs frequency, duration, intensity has increased over the ARB. The decrease in the activity over BoB is observed in November due to a significant decrease in mid-level relative humidity. The frequency and duration of TCs in May, June, and October have increased significantly over ARB. An increase in SST, TCHP, surface latent heat flux (ocean to atmosphere), mid-level RH, and MSE (950-150 hPa) are significantly correlated to the duration of TCs over ARB. All of these analyses reveal changes in the local dynamical and thermodynamical characteristics that contribute to changes in tropical cyclone activity over the north Indian Ocean. In the future, large-scale variability and circulation changes that contribute to these local changes will be investigated.

Acknowledgements IITM is fully funded by the Ministry of Earth Sciences, Government of India. We thank JTWC for the best track dataset, NOAA for the OISST data set, NCEP-GODAS for ocean subsurface monthly temperature data utilized to calculate TCHP. High resolution ERA5 monthly mean reanalysis data is also acknowledged with thanks. All datasets used for this study are freely available online.

References

Alam MM, Hossain MA, Shafee S (2003) Frequency of Bay of Bengal cyclonic storms and depressions crossing different coastal zones. Int J Climatol 23:1119–1125. https://doi.org/10.1002/joc.927

Baburaj PP, Abhilash S, Mohankumar K, Sahai AK (2020) On the epochal variability in the frequency of cyclones during the pre-onset and onset phases of the monsoon over the north Indian Ocean. Adv Atmos Sci 37:634–651. https://doi.org/10.1007/s00376-020-9070-5

Balaguru K, Taraphdar S, Leung LR, Foltz GR (2014) Increase in the intensity of postmonsoon Bay of Bengal tropical cyclones. Geophys Res Lett. https://doi.org/10.1002/2014GL060197

Balaji M, Chakraborty A, Mandal M (2018) Changes in tropical cyclone activity in north Indian Ocean during satellite era (1981–2014). Int J Climatol 38:2819–2837. https://doi.org/10.1002/joc.5463

Bell SS, Chand SS, Tory KJ et al (2020) North Indian Ocean tropical cyclone activity in CMIP5 experiments: future projections using a model-independent detection and tracking scheme. Int J Climatol. https://doi.org/10.1002/joc.6594

Bhat GS (2003) Measurement of air–sea fluxes over the Indian Ocean and the Bay of Bengal. J Clim 1:12. https://doi.org/10.1175/1520-0442(2003)016%3c0767:MOASFO%3e2.0.CO;2

Bhatia K, Vecchi G, Murakami H et al (2018) Projected response of tropical cyclone intensity and intensification in a global climate model. J Clim. https://doi.org/10.1175/JCLI-D-17-0898.1

Bhatla R, Raj R, Mall RK (2020) Tropical cyclones over the north Indian Ocean in changing climate. In: Srivastava PK, Singh SK, Mohanty UC, Tad M (eds) Techniques for disaster risk management and mitigation. Wiley, New York, pp 63–76

Bister M, Emanuel KA (2002) Low frequency variability of tropical cyclone potential intensity 1. Interannual to interdecadal variability. J Geophys Res Atmos. https://doi.org/10.1029/2001JD000776

Camargo SJ, Sobel AH (2005) Western North Pacific tropical cyclone intensity and ENSO. J Clim 18:2996–3006. https://doi.org/10.1175/JCLI3457.1

Chu JH, Sampson CR, Levine AS, Fukada E (2002) The JointTyphoon Warning Center tropical cyclone best-tracks 1945–2000. Washington, DC

Daloz AS, Camargo SJ (2018) Is the poleward migration of tropical cyclone maximum intensity associated with a poleward migration of tropical cyclone genesis? Clim Dyn 50:705–715. https://doi.org/10.1007/s00382-017-3636-7

Deo AA, Ganer DW (2015) Tropical cyclone activity over the Indian Ocean in the warmer climate. Int J Sci Res 4:880–886. https://doi.org/10.1007/978-94-007-7720-0

Deo AA, Ganer DW, Nair G (2011) Tropical cyclone activity in global warming scenario. Nat Hazards 59:771–786. https://doi.org/10.1007/s11069-011-9794-8

Dube SK, Rao AD, Sinha PC et al (1997) Storm surge forecasting in the Bay of Bengal and Arabian Sea. Mausam 48:283–304

Elsner JB, Kossin JP, Jagger TH (2008) The increasing intensity of the strongest tropical cyclones. Nature 455:92–95. https://doi.org/10.1038/nature07234

Emanuel K (2005) Increasing destructiveness of tropical cyclones over the past 30 years. Nature 436:686–688. https://doi.org/10.1038/nature03906

Emanuel KA, Neelin JD, Christopher S (1994) On large-scale circulations in convecting atmospheres. Q J R Meteorol Soc 120:1111–1143. https://doi.org/10.1002/qj.49712051902

Evan AT, Camargo SJ (2011) A climatology of Arabian Sea cyclonic storms. J Clim 24:140–158. https://doi.org/10.1175/2010JCLI3611.1

Evan AT, Kossin JP, Chung CE, Ramanathan V (2011) Arabian Sea tropical cyclones intensified by emissions of black carbon and other aerosols. Nature. https://doi.org/10.1038/nature10552

Galarneau TJ, Davis CA (2013) Diagnosing forecast errors in tropical cyclone motion. Mon Weather Rev. https://doi.org/10.1175/MWR-D-12-00071.1

Goldenberg SB, Landsea CW, Mestas-Nuñez AM, Gray WM (2001) The recent increase in Atlantic hurricane activity: causes and

implications. Science 293:474–479. https://doi.org/10.1126/science.1060040
Grodsky SA, Bentamy A, Carton JA, Pinker RT (2009) Intraseasonal latent heat flux based on satellite observations. J Clim 22:4539–4556. https://doi.org/10.1175/2009JCLI2901.1
Hersbach H, Bell B, Berrisford P et al (2020) The ERA5 global reanalysis. Q J R Meteorol Soc. https://doi.org/10.1002/qj.3803
Joseph S, Ravichandran M, Kumar BP, Jampana RV, Weiqing H (2017) Ocean atmosphere thermal decoupling in the Eastern Equatorial Indian Ocean. Clim Dyn 49:575–594. https://doi.org/10.1007/s00382-016-3359-1
Kim S-H, Moon I-J, Chu P-S (2020) An increase in global trends of tropical cyclone translation speed since 1982 and its physical causes. Environ Res Lett. https://doi.org/10.1088/1748-9326/ab9e1f
Klotzbach PJ (2006) Trends in global tropical cyclone activity over the past twenty years (1986–2005). Geophys Res Lett 33:1984–1987. https://doi.org/10.1029/2006GL025881
Knaff JA, Sampson CR, DeMaria M (2005) An operational statistical typhoon intensity prediction scheme for the western North Pacific. Weather Forecast 20:688–699. https://doi.org/10.1175/WAF863.1
Knutson T, Camargo SJ, Chan JCL et al (2020) Tropical cyclones and climate change assessment: part 2: projected response to anthropogenic warming. Bull Am Meteorol Soc 101:E303–E322. https://doi.org/10.1175/BAMS-D-18-0189.1
Kotal SD, Kundu PK, Roy Bhowmik SK (2009) Analysis of cyclogenesis parameter for developing and nondeveloping low-pressure systems over the Indian Sea. Nat Hazards 50:389–402. https://doi.org/10.1007/s11069-009-9348-5
Leipper DF, Volgenau LD (1972) Hurricane heat potential of the Gulf of Mexico. J Phys Oceanogr 2(3):218–224
Lin II, Wu CC, Pun IF, Ko DS (2008) Upper-ocean thermal structure and the Western North Pacific category 5 typhoons. Part I: Ocean features and the category 5 typhoons' intensification. Mon Weather Rev 136:3288–3306. https://doi.org/10.1175/2008MWR2277.1
Marquet P (2015) On the computation of moist-air specific thermal enthalpy. Q J R Meteorol Soc 141:67–84. https://doi.org/10.1002/qj.2335
Mittal R, Tewari M, Radhakrishnan C et al (2019) Response of tropical cyclone Phailin (2013) in the Bay of Bengal to climate perturbations. Clim Dyn 53:2013–2030. https://doi.org/10.1007/s00382-019-04761-w
Mohapatra M, Adhikary S (2011) Modulation of cyclonic disturbances over the North Indian ocean by madden—Julian oscillation. Mausam 62:375–390
Mohapatra M, Vijay Kumar V (2017) Interannual variation of tropical cyclone energy metrics over North Indian Ocean. Clim Dyn 48:1431–1445. https://doi.org/10.1007/s00382-016-3150-3
Mohapatra M, Bandyopadhyay BK, Tyagi A (2014) Construction and quality of best tracks parameters for study of climate change impact on tropical cyclones over the north Indian Ocean during satellite era. In: Mohanty UC, Mohapatra M, Singh OP et al (eds) Monitoring and prediction of tropical cyclones in the Indian Ocean and Climate Change. Springer, Dordrecht, pp 3–17
Murakami H, Sugi M, Kitoh A (2013) Future changes in tropical cyclone activity in the north Indian Ocean projected by the new high-resolution MRI-AGCM. Clim Dyn 40:1949–1968. https://doi.org/10.1007/978-94-007-7720-0_6
Murakami H, Vecchi GA, Underwood S (2017) Increasing frequency of extremely severe cyclonic storms over the Arabian Sea. Nat Clim Chang 7:885–889. https://doi.org/10.1038/s41558-017-0008-6
Murakami H, Delworth TL, Cooke WF et al (2020) Detected climatic change in global distribution of tropical cyclones. Proc Natl Acad Sci USA 117:10706–10714. https://doi.org/10.1073/pnas.1922500117
Neelin JD, Held ID (1987) Modeling tropical convergence based on the moist static energy budget. Mon Weather Rev 115:3–12. https://doi.org/10.1175/1520-0493(1987)115%3c0003:MTCBOT%3e2.0.CO;2
Ng EKW, Chan JCL (2012) Interannual variations of tropical cyclone activity over the north Indian Ocean. Int J Climatol 32:819–830. https://doi.org/10.1002/joc.2304
Ohring G, Gruber A (1983) Satellite radiation observations and climate theory. Adv Geophys 25:237–304. https://doi.org/10.1016/S0065-2687(08)60175-2
Pokhrel S, Dutta U, Rahaman H, Chaudhari H, Hazra A, Saha SK, Veeranjaneyulu C (2020) Evaluation of different heat flux products over the tropical Indian Ocean. Earth Space Sci 7:e2019EA000988. https://doi.org/10.1029/2019EA000988
Rajeevan M, Srinivasan J, Niranjan Kumar K et al (2013) On the epochal variation of intensity of tropical cyclones in the Arabian Sea. Atmos Sci Lett. https://doi.org/10.1002/asl2.447
Rappin ED, Nolan DS, Emanuel KA (2010) Thermodynamic control of tropical cyclogenesis in environments of radiative-convective equilibrium with shear. Q J R Meteorol Soc 136:1954–1971. https://doi.org/10.1002/qj.706
Reddy JP, Sriram D, Gunthe SS et al (2021) Impact of climate change on intense Bay of Bengal tropical cyclones of the post-monsoon season: a pseudo global warming approach. Clim Dyn 56:2855–2879. https://doi.org/10.1007/s00382-020-05618-3
Reynolds RW, Smith TM, Liu C et al (2007) Daily high-resolution-blended analyses for sea surface temperature. J Clim 20:5473–5496. https://doi.org/10.1175/2007JCLI1824.1
Roxy MK, Dasgupta P, McPhaden MJ et al (2019) Twofold expansion of the Indo-Pacific warm pool warps the MJO life cycle. Nature 575:647–651. https://doi.org/10.1038/s41586-019-1764-4
Schreck CJ, Molinari J, Mohr KI (2011) Attributing tropical cyclogenesis to equatorial waves in the western north pacific. J Atmos Sci 68:195–209. https://doi.org/10.1175/2010JAS3396.1
Sharma N, Ali MM (2014) Importance of ocean heat content for cyclone studies. Oceanography 2:124. https://doi.org/10.4172/2332-2632.1000124
Shay LK, Goni GJ, Black PG (2000) Effects of a warm oceanic feature on Hurricane Opal. Mon Weather Rev 128:1366–1383. https://doi.org/10.1175/1520-0493(2000)128%3c1366:eoawof%3e2.0.co;2
Singh OP, Ali Khan TM, Rahman MS (2000) Changes in the frequency of tropical cyclones over the north Indian Ocean. Meteorol Atmos Phys 75:11–20. https://doi.org/10.1007/s007030070011
Singh OP, Khan TMA, Rahman MS (2001) Has the frequency of intense tropical cyclones increased in the north Indian Ocean? Curr Sci 80:575–580
Singh K, Panda J, Rath SS (2019a) Variability in landfalling trends of cyclonic disturbances over North Indian Ocean region during current and pre-warming climate. Theor Appl Climatol 137:417–439. https://doi.org/10.1007/s00704-018-2605-3
Singh K, Panda J, Sahoo M, Mohapatra M (2019b) Variability in tropical cyclone climatology over north Indian Ocean during the period 1891 to 2015. Asia Pac J Atmos Sci 55:269–287. https://doi.org/10.1007/s13143-018-0069-0
Srivastav AK, Sinha Ray KC, De US (2000) Trends in the frequency of cyclonic disturbances and their intensification over Indian Seas. Mausam 51:113–118
Suneeta P, Sadhuram Y (2018) Tropical cyclone genesis potential index for Bay of Bengal during peak post-monsoon (October–November) season including atmosphere–ocean parameters. Mar Geod. https://doi.org/10.1080/01490419.2017.1394404
Wang S, Toumi R (2021) Recent migration of tropical cyclones toward coasts. Science 371:514–517. https://doi.org/10.1126/science.abb9038

Wang B, Xu S, Wu L (2012) Intensified Arabian Sea tropical storms. Nature 489:E1–E2. https://doi.org/10.1038/nature11470

Webster PJ, Holland GJ, Curry JA, Chang HR (2005) Atmospheric science: changes in tropical cyclone number, duration, and intensity in a warming environment. Science 309:1844–1846. https://doi.org/10.1126/science.1116448

Zhang K, Randel WJ, Fu R (2017) Relationships between outgoing longwave radiation and diabatic heating in reanalyses. Clim Dyn 49:2911–2929. https://doi.org/10.1007/s00382-016-3501-0